AD-A177 103 MULTITECHNIQUE STUDIES ON FRETTING FATIGUE: INFLUENCE OF SURFACE TREATMENT(U) BUNDESANSTALT FUER MATERIALPRUEFUNG BERLIN (GERMANY F R) H SANDER NOV 86 1/1

UNCLASSIFIED R/D-4038-AN DAJA45-83-C-0019 F/G 20/11 NL

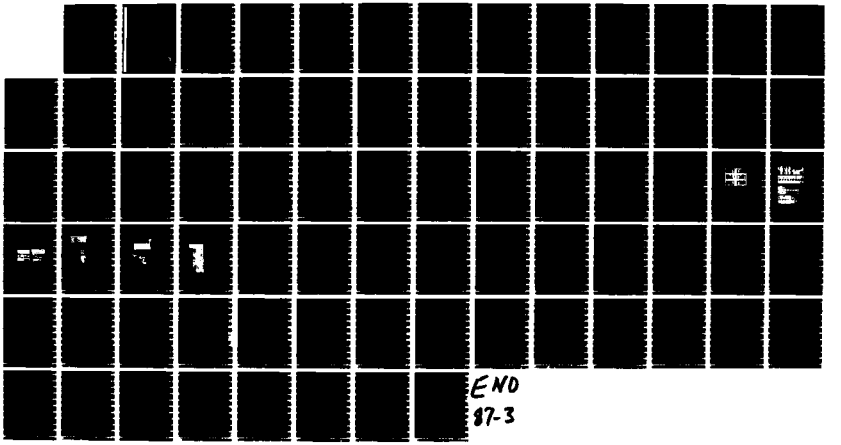

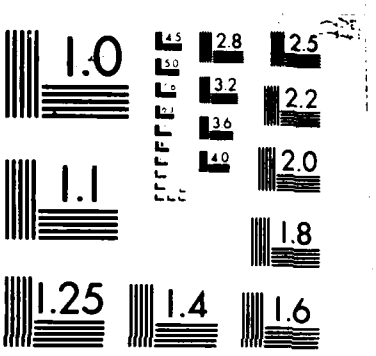

(10)

AD R+D 4038-AN

Multitechnique Studies on Fretting Fatigue: Influence of Surface Treatment

Final Technical Report

by

Harro Sander

November 1986

United States Army

EUROPEAN RESEARCH OFFICE OF THE U.S. ARMY

London England

Contract Number DAJA 45-83-C-0019

Bundesanstalt für Materialprüfung Berlin (BAM)

R&D 4038-AN

REPORT DOCUMENTATION PAGE

READ INSTRUCTIONS BEFORE COMPLETING FORM

1. REPORT NUMBER

2. GOVT ACCESSION NO. ADA177103

3. RECIPIENT'S CATALOG NUMBER

4. TITLE (and Subtitle)
Multitechnique Studies on Fretting Fatigue: Influence of Surface Treatment

5. TYPE OF REPORT & PERIOD COVERED
Final Technical Report
Jan 83 - Mar 86

6. PERFORMING ORG. REPORT NUMBER

7. AUTHOR(s)
Harro Sander

8. CONTRACT OR GRANT NUMBER(s)
DAJA45-83-C-0019

9. PERFORMING ORGANIZATION NAME AND ADDRESS
Bundesanstalt für Materialprüfung Berlin (BAM)
Unter den Eichen 87
D - 1000 Berlin 45, Germany

10. PROGRAM ELEMENT, PROJECT, TASK AREA & WORK UNIT NUMBERS
61102A
1L161102BH57-06

11. CONTROLLING OFFICE NAME AND ADDRESS
USARDSG-UK
Box 65
FPO NY 09510-1500

12. REPORT DATE
November 1986

13. NUMBER OF PAGES
73

14. MONITORING AGENCY NAME & ADDRESS(if different from Controlling Office)

15. SECURITY CLASS. (of this report)
Unclassified

15a. DECLASSIFICATION/DOWNGRADING SCHEDULE

16. DISTRIBUTION STATEMENT (of this Report)
Approved for Public Release; distribution unlimited

17. DISTRIBUTION STATEMENT (of the abstract entered in Block 20, if different from Report)

18. SUPPLEMENTARY NOTES

19. KEY WORDS (Continue on reverse side if necessary and identify by block number)
Fretting fatigue, surface treatment, surface roughness, polishing, shaping, fatigue cracks, contact pressure, contact resistance, contact temperature, normal force, friction force, linear wear rate, shear stress, crack detection, magnetic induction.

20. ABSTRACT (Continue on reverse side if necessary and identify by block number)
In the experimental program a specially constructed apparatus was used to simulate conditions at the faying surfaces in a structural joint. Fretting fatigue tests were carried out on 34CrNiMo6/100Cr6 steels using stress ratios from the range of finite endurance. Two methods of surface treatments are used: polishing and shaping. Two directions of each surface treatment are considered: parallel and perpendicular to the sliding direction.
The results are compared to baseline tests on the same material without

DD FORM 1 JAN 73 1473 EDITION OF 1 NOV 65 IS OBSOLETE

20. Contd.

fretting and are discussed in terms of the effect of surface roughness and normal force.

Abstract

In the experimental program a specially constructed apparatus was used to simulate conditions at the faying surfaces in a structural joint. Fretting fatigue tests were carried out on 3[illegible]NiMo6/100Cr6 steels using stress ratios from the range of finite endurance. Two methods of surface treatments are used: polishing and shaping. Two directions of each surface treatment are considered: parallel and perpendicular to the sliding direction.

The results are compared to baseline tests on the same material without fretting and are discussed in terms of the effect of surface roughness and normal force.

Keywords:

Fretting fatigue, surface treatment, surface roughness, polishing, shaping, fatigue cracks, contact pressure, contact resistance, contact temperature, normal force, friction force, linear wear rate, shear stress, crack detection, magnetic induction.

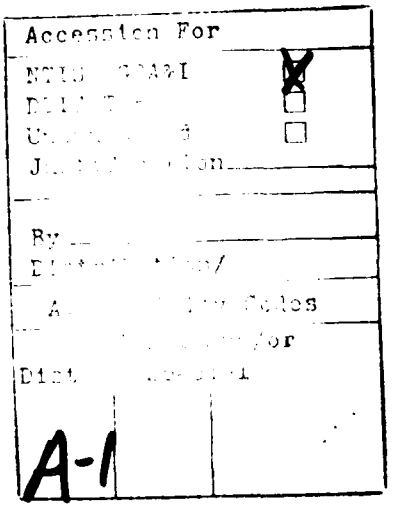

Table of Contents page

List of Illustrations page

List of Illustrations page

List of Illustrations page

List of Illustrations page

List of Illustrations page

List of Illustrations page

1. Introduction

Fretting fatigue is a failure mechanism caused by a structural member experiencing fatigue loading while at the same time undergoing a tribological loading due to another body coming into contact under a clamping load. Fretting fatigue initiated damage occurs at the contacting surfaces of components which although nominally at rest relative to each other, are subjects of vibrations. It is caused by repeated slipping of the surfaces over part of their mutual contact area. This movement can, at or near certain points of contact between the faces, induce fatigue stresses of sufficient intensity to cause cracking. Thus the combination of frictional stress and repeated stress accellerates crack initiation as well as crack propagation. The net result of fretting fatigue is to introduce a reduction in fatigue life at a given stress and also to eliminate the fatigue limit or apparent fatigue limit. These effects are

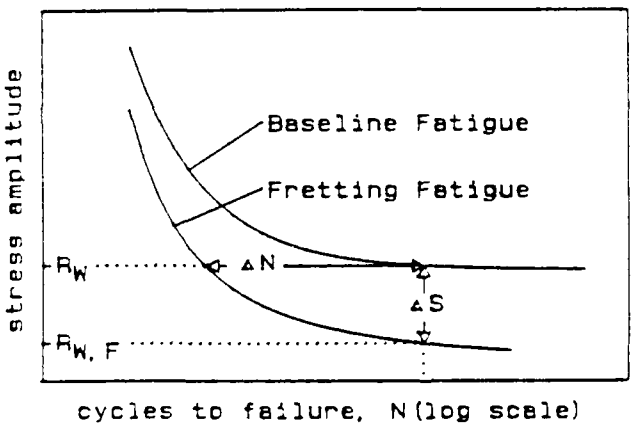

Fig.1 - Schematic illustrating the potential reduction in fatigue life brought about by additional fretting.

illustrated diagrammatically in Fig.1. The fatigue strength Rw at a given endurance (10exp7) is lowered by the rate dS to the fretting fatigue strength Rw,f. dN is the decrease of the endurance at a stress level

of the amount of the fatigue strength. The relation between the fatigue strength Rw and the fretting fatigue strength Rw,f can be formularized by the equation $R_{w,f} = R_w - dS(p1,p2,...)$. The fretting fatigue strength is influenced by factors affecting normal fatigue but it additionally involves those parameters p1, p2, ... which characterize the tribological system. Thus the fretting fatigue strength is no material specific quantity, as the fatigue strength, but it is a quality of the tribological system which can also be nominated as a pairing feature of components.

Failures due to fretting fatigue have become increasingly numerous. Fretting fatigue in technical systems is recognized as a major source of failure in establishing and maintaining structural integrity. It frequently leads to high maintenance and inspection costs, increasing loss time and excessive retrofit requirements. Thus, durability and safety consideration relate to the presence of fretting fatigue. The reasons for the increasing incedence of such failures are the greater demands placed on components, closer tolerances, and the scaling up of existing plant to a point where movement at mating surfaces exceeds the critical amplitude for fretting /1,2,3/.

There are numerous engineering situations where the requirements for the occurrence of fretting fatigue may be encountered /4/. One typical case is the contact region of a member which is press or shrink fitted to a loaded shaft, such as the wheel-on-axle assembly as shown in Fig.2. Practical examples of this type of assembly are a railway-wagon axle having a pressed-on wheel, a build-up steam turbine rotor consisting of a shaft with a shrunk-on disc, and a gear flange fitted on a shaft.

When the axle is loaded cyclically it is subject to bending stresses which deform the axle. During rotation of the axle each point in the surface goes through successive cycles of compressive and tensile stress (in practice such assemblies are generally subjected to rotating bending stresses). If then the shear stress in the mating interface exceeds the

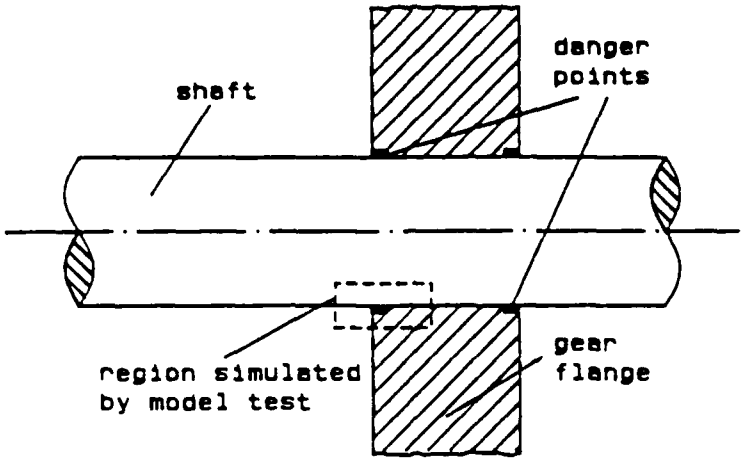

Fig.2 - Schematic diagram of a wheel-on-axle assembly illustrating the position of frequently observed fretting damage.

friction stress local movement occurs between the sleeve and the axle. The greatest movement occurs at the extremities of the sleeve. The damage of fretting in these conditions is the initiation of fatigue cracks in the axle so that fatigue strength of the assembly is found to be less than that of the shaft itself. Generally these fatigue cracks are found to occur on the surface of the shaft in areas of fretting just inside the wheel seat.

Returning now to the equation of the foregoing page, the challenge of fretting fatigue is considerably complex because of numerous factors pi influencing the processes of the contacting surfaces. Since fretting fatigue cracks frequently start at or near the interface of the contacting bodies, the surface condition is an important consideration in fretting fatigue life. Accordingly, any alteration in surface properties must bring about a change in the fretting fatigue properties. As mating surfaces of structural parts are treated in a special way, it is important for service life whether the surface treatment decreases or increases the resistance against fretting fatigue initiated damage.

The experimental investigation described in this paper was therefore designed to examine the fretting fatigue behaviour of steel specimens, with specific reference to the effects of mechanical surface treatments. Two types of surface finishes were studied: Smooth surfaces produced by grinding and rough surfaces made by shaping. Within each group two directions of surface treatment were considered, parallel and perpendicular to the slip direction. The results are compared to baseline tests on the same material and with the same surface treatment.

2. Experimental details

2.1 Experimental approach

The investigation of the influence of different surface finishes on the fretting fatigue process is related to the wheel-on-axle assembly as shown in Fig.2. The selected experimental way is the model test, were the fretting fatigue conditions occurring in practice were simulated. The specimens are then to understand as geometrically abstracted parts. The

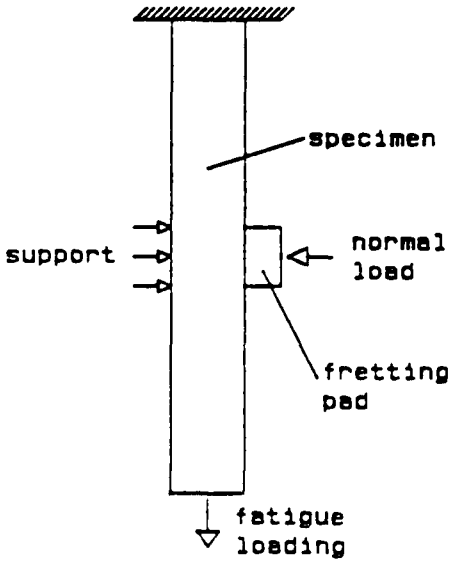

Fig.3
Schematic diagram of fretting fatigue loading.

tribological system according to the practical press fit is shown in Fig.3. It contains only those parts of the tecnnical system which immediately take part in the fretting fatigue process, thoughtly separated from the rest of the system. This region is marked in Fig.2 by the dotted lined rectangle. The fatigue loaded specimen corresponds to the shaft whereas the fretting pad which is presseo against the specimen by normal force corresponds to the flange of the simulated system. The normal force related to the contact area simulates the clamping pressure of the press fitted assembly.

2.2 Apparatus

The loading system is built by a servo hydraulic testing machine to apply axial fatigue loads and a fretting arrangement in order to induce fretting in addition to the axial fatigue loads. A diagram of the experimental apparatus is shown in Fig.4. The fretting arrangement is based on the bridge principle with one foot of the bridge anchored on the upper specimen grip which is fixed. The unfixed lower end of the bridge which carries the cylindrical fretting pad touches the midsection of the specimens front-side. The relative movement between the fatigue loaded specimen and the stationary fretting pad originates from the push-pull loading and is defined by the equation indicated in Fig.4. The amplitude s of the slip movement s is proportional to the amplitude Ao of the push-pull loading. The factor of proportionality is determined by the dimensions of the specimen and the fretting device. A change of the slip amplitude caused by the fatigue loading is only possible by a variation of the length of the fretting bridge which can be done by means of distance rings mounted between the anchored foot of the bridge and the fixed grip. Using strain gauges attached to thin-walled sections of the fretting arm, both tangential force and linear wear rate can be monitored throughout the duration of an experiment.

The midsection of the specimen is supported from the backside by a PTFE block to prevent bending and fretting on the backside of the specimen.

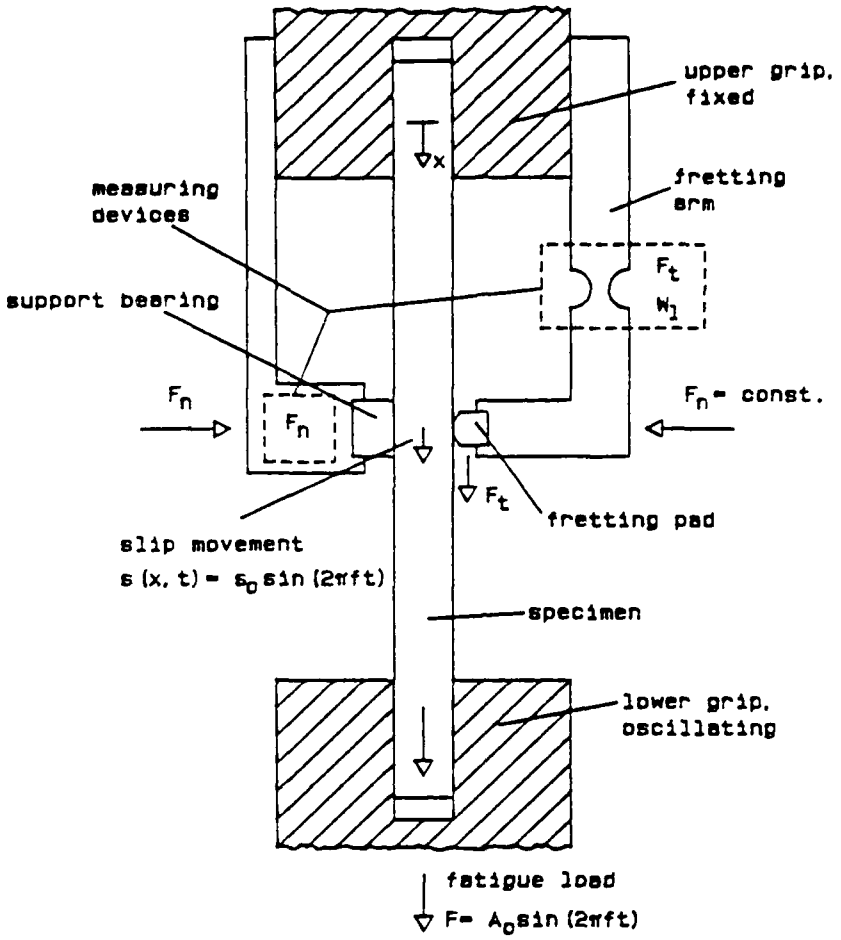

Fig.4 - Principle arrangement of the apparatus for carrying out fretting fatigue tests in push-pull mode.

The fretting pad and the support bearing are pressed against the fatigue specimen by the normal force Fn, which is generated by a servo controlled loading system. This electromagnetically driven device replaces the hitherto used proving ring. The advantage of the active force generation is that the normal force remains constant during the experimental run and does not depend on the wear rate which is the case with the proving ring.

A diagram of the normal force generation is shown in Fig.5. Fretting pad and bearing support are pressed onto the specimen by means of a flexible metal rope which runs over a deflection roller and is pulled by an electromagnet. The PTFE block of the support bearing is mounted on a rigid bending spring which is strain gauged to monitore the normal force. A power amplification is required to increase the value of this generated signal to drive the electro magnet. A constant level control unit is included in the system to permit, in association with a feedback loop, the detection of any sudden change in the value of the normal force and to respond immediately to maintain the set level of the normal force.

A complete description of the apparatus, especially of the fretting device, has been published earlier /5/.

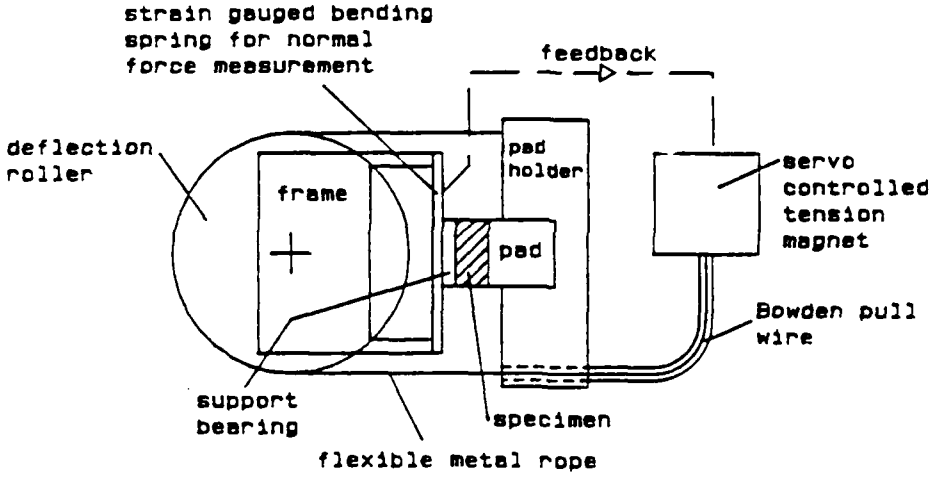

Fig.5 - Diagram of the normal force generator.

2.3 Specimen and material

Since the practical system which will be simulated by model tests is the system gear flange/shaft, the shaft steel identified by the German Standard W.No. 1.6582 (34 CrNiMo 6) was chosen as material

for specimen and the bearing steel German Standard W.No. 1.3505 (100 Cr 6; AISI 52100) was selected as material for fretting pads. The specimen and fretting pad configurations are shown in Fig.6. The fretting pad has two opposing cylindrical faces so that each pad can be utilized twice in fretting fatigue tests.

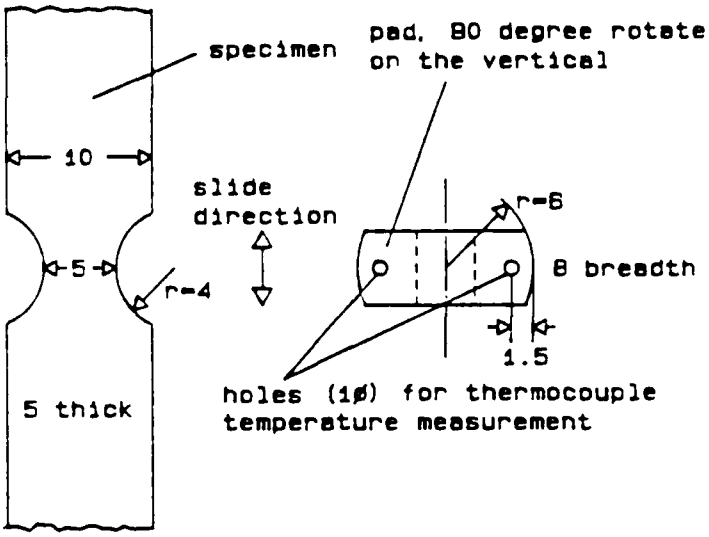

Fig.6 - Shape and dimensions of the fretting fatigue specimen and the fretting pad used for investigation (dimensions in mm).

The flat specimens and the cylindrical pads were machined from cylindrical rods of different diameters in the range of 20 mm to 40 mm. Then the coarse adjustment of the surface finish followed. The smooth surfaces were made by grinding whereas the rougher surfaces were produced by shaping.

After being machined all specimens and fretting pads were heat treated in the same manner as applicated to the parts in practice.

During the experimental run one of the two cylindrical faces of the fretting pad is pressed against the specimen by normal force. The contact position is the midsection of the notch of the specimen. Initially the zone of contact has the line shape.

After the heat treatment the specimens and pads were cleaned from forge and then polished with emery paper to produce the desired surface finish.

2.4 Test procedure

To test the influence of different surface finishes of steel specimens on their fatigue and fretting fatigue behaviour comparative tests with specimens of the same design were conducted: uniaxial fatigue loading on one side and uniaxial fatigue loading with superimposed fretting on the other side.

The fatigue tests were performed with a second servohydraulic testing machine of the same type as the one used to conduct the fretting fatigue tests.

Both types of experiments were carried out simultaneously in laboratory environment under similar atmospheric conditions. The laboratory temperature was 21 C and the relative humidity was in the range of 30...50 %.

A sine waveform was used for alternating tension and compression loading. All tests were conducted at a frequency of 20 Hz.

2.4.1 Fatigue tests

In addition fatigue tests were required to establish control data points for reference against later fretting fatigue results. To determine the fatigue properties a batch of specimens were subjected to a cyclic stress of constant amplitude throughout their lifes. The tests were carried out at stress levels giving failure after an endurance of less than 10exp7 cycles. The results will be usually plotted on the familiar S/N or Woehler curve (i.e. stress versus the number of cycles to failure, usually plotted on a logarithmic scale). Then each of the received S/N curves belongs to a batch of specimens with a definite surface finish.

2.4.2 Fretting fatigue tests

Fretting fatigue tests were conducted on definite surface finishes of the shaft steel specimens to determine variations in fretting fatigue lives due to surface condition differences. These data were then compared with the baseline fatigue data for each type of surface finish.

The test conditions were set by the following experimental parameters at the beginning of each test:

Fatigue loading F : 400 - 600 MPa
Normal load, Fn : 50, 100 or 200 N
Frequency, f : 20 Hz

The measuring parameters of the running tests and their ranges were:

Number of cycles, N : 1 - 10,000,000 cycles
Friction force, Ft : 0 - 200 N
Linear ware rate, Wl: 0 - 150 μm

Electrical resistance, R : 0 - infinity Ohm
Temperature of the specimen, T: 20 - 50 C
Magnetic induction voltage, U : 5 - 30 mV

The slip amplitude depends on the applied axial loads. For the geometrical conditions of the experimental equipment and the specimen the amplitude of movement at the point of contact is determined by the equation s[μm] = 0.156 S [MPa]. Thus the slip movement referred to the applied axial load was:

Slip movement, s: 0 - 120 μm

The magnetic induction voltage, which is measured by a coil wound close to the specimen, was utilized as a crack growth indicator. For this purpose each specimen was magnetized to saturation in the sense of length before the beginning of the test.

During the test run the variables were measured with an electronic data measurement and acquisition system after fixed numbers of loading cycles. Software was developed to control the fretting fatigue

experiment according to parameters specified by the operator. The digital data were stored on magnetic tape data cartridges after preliminary data processing. At the end of each test the mentioned test quantities were plotted as a function of the number of loading cycles.

2.5 Measuring technique

2.5.1 Measurement of linear wear rate

The linear wear rate was determined continuously throughout each test by measuring the change of distance between fretting pad and specimen by strain gauges mounted on the fretting arm. This method of measurement gives the summation -for both pad and specimen- of all material lost below the original datum surface. A potential error to which this method is susceptible is, that it cannot distinguish between the real scar debth and the apparent debth resulting from the presence of trapped fretting debris.

To separate the amounts of wear resulting from the specimen and the pad the linear wear rate of the pad was additionally determined from its weight loss and from the dimensions of its wear scar. The calculations are based on the cylindrical cap approximation which was applied to the wear scar geometry:

The fretting pads were weighed before and after each fretting fatigue test with a microbalance. The linear wear rate of the pad was then calculated according to one of the relationships (2) or (3) of Fig.7. The more simple equation (3) is a good approximation with an accuracy better than 2 %. As the wear volume under the experimental conditions was very small weight loss measurements involved some error.

To deduce more wear rate data of the pad from the wear scar dimensions the width of the flat wear scar was measured in oscillation direction by a microscop. The linear wear rate was computed with the exact formula (1) of Fig.7.

Additionally, information about the wear mechanism can be obtained from comparison of the different

wear rate types completed by microscopic investigation of the surface properties in the region of the fretting mark.

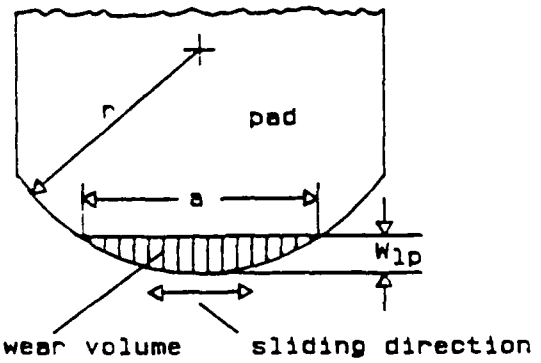

$$W_{1p} = r - \sqrt{r^2 - a^2/4} \qquad (1)$$

$$\Delta m, bg = r\sqrt{W_{1p}(2r + W_{1p}/3)} - (r - W_{1p})\sqrt{W_{1p}(2r - W_{1p})} \qquad (2)$$

$$W_{1p}\,[\mu m] = 30.64\,(\Delta m\,[mg])^{0.68} \qquad (3)$$

Fig.7 - Simplified wear scar for the estimation of the linear wear rate of the pad.
r: pad radius, a: scar diameter in the oscillation direction and b: scar diameter perpendicular to it, ϱ: density of the pad material, Δm: weight loss, Wlp: linear wear rate of the pad.

2.5.2 Measurement of friction force

The tangential frictional force Ft was measured continuously throughout every experiment by means of four strain gauges mounted on the fretting pad support. The output of the strain gauge bridge was amplified and displayed as a trace on an oscilloscope so that the force-time and the force-displacement characteristics can be continuously observed.

The actual value of the friction coefficient was calculated from the ratio μ = Ft/Fn.

2.5.3 Determination of slip

The real interfacial slip movement is no free adjustable experimental parameter, it is dependend upon the alternating stress of the specimen and the amount of the applied normal force. The slip amplitude, which is always smaller than the stress induced movement s of the specimen at the point of contact (see 2.4.2), can be taken from the friction force-displacement hysteresis (see 2.5.4).

2.5.4 Ft-s hysteresis loop measurements

A complete friction force - displacement hysteresis loop was determined by gathering 50 data points during one loading cycle. To prevent parasitic oscillations of the fretting device due to stic slip, the frequency of the fatigue load function was lowered for one cycle from 20 to 1 Hz.

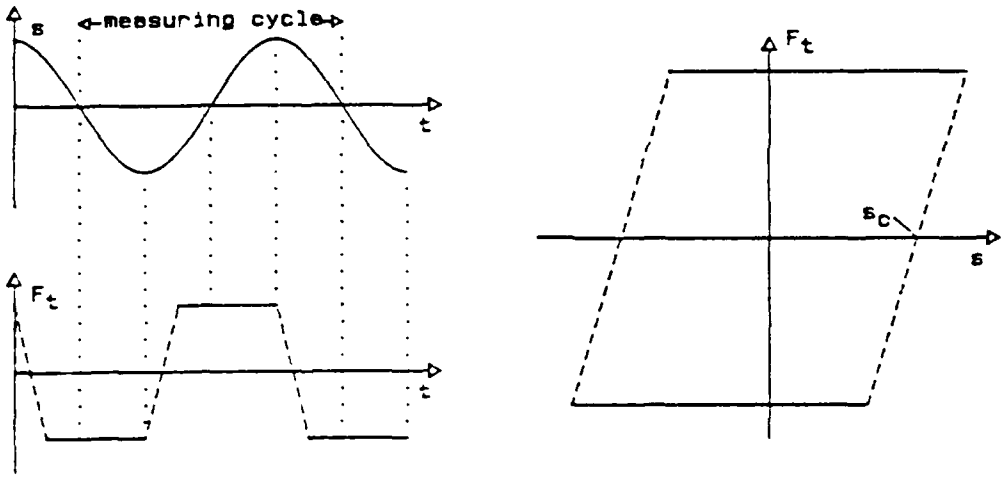

—— periods of slip at interface, v≠ 0

---- periods of virtually no slip at interface, v=0

Fig.8 - Schematic representation of the friction force-displacement hysteresis. s: displacement, Ft: friction force, s : slip amplitude, t: time, v: speed of movement.

From this hysteresis loop special parameters can be arrived, such as maximum friction force, slip amplitude, frictional energy dissipation, ...

Fig.8 shows in a schematic diagram the correlation of the cyclic strain of the specimen with variations of the frictional force at the fretting interface. The upper curve on the left side shows the sinusoidal cyclic strain of the specimen while the lower curve is a measure of the frictional force on the fretting interface. The frictional force passes through two distinct regimes. The first which is marked by dotted lines is the one where the slope of the frictional force curve reverses sign and changes rapidly for a period of time. The second which is marked by a solid line is a period of relatively constant frictional force. The first regime is a period during which the interface is not sliding significantly because the tangential force is less than the critical value to initiate sliding. The second regime is the period in which interfacial sliding occurs because the continuing straining of the specimen has resulted in a tangential force greater than the static frictional force. As a result of these two regimes the friction force-displacement hysteresis has the shape of an trapezoid (right side of Fig.8).

2.5.5 Measurement of electrical contact resistance

The contact resistance was determined by two d.c. methods at low voltage and current (maximum values, 5v and 1 mA) so as not to cause heating or electrical breakdown of insulating films that may be present in the interface.

The first one using the resistance measurement capability of a digital voltmeter takes the mean value of the contact resistance integrated over the time of one loading cycle. The so gained resistance gives information about variation of the contact conditions with number of cycles.

The second measuring method gives the instantaneous value of the contact resistance as a function of pad location traced during one half cycle. During the measuring time, while the frequency is lowered to 1 Hz in order to prevent parasitic oscillations, the

fretting pad moves relatively to the specimen from one end of the fretting mark to the other. The electrical contact resistance in the contact zone between the sliding specimen and the stationary pad is detected by a fast measurement of the voltage drop when passing a d.c. current through the contact. The resistance as a function of the displacement was gathered by 400 measuring points, that means about two points per micrometer. Preliminary tests have shown, that 400 data points are sufficient to describe the fluctuations of the resistance which appear during the movement of the pad across the wear track. From these data, information of the wear process and of the action of wear debris which appear within one half loading cycle can be obtained /6/.

2.5.6 Temperature measurement

The fretting motion is accompanied by consumption of energy and frictional heating. For the experimental measurement of the interface temperature rise during fretting iron-constantan (type J) thermocouples were imbedded into the fretting pad as near as possible to the contact surface as indicated in Fig.6 to sense an average value. The temperature of the reference junction is computed using the resistance measurement of a thermistor located with the junction.

As a reference the temperature of the shaft of the specimen is determined by a second thermocouple.

2.5.7 Magnetic induction measurement

The method of magnetic induction measurement was used for continuous monitoring the status of damage of the specimens running under conditions where fretting fatigue cracks are likely to occur. The method is shown to be capable of detecting the nucleation and the growth of the cracks. It is also possible to use the detected signal to shut down the testing machine in order to facilitate microscope examination of the flaws to be carried out as soon as they are first detected.

The experimental device is very simple as it consists of a couple of pick-up coils similar to a Helmhotz coil wound close to the specimen, each one at one side of the specimen's notch. The fretting pad and the support bearing are acting through the gap between the two coils. The total number of turns is 300.

The basis of the magnetic crack growth detection consists in detecting the change of the flux through the ferromagnetic specimen, which is caused by surface and subsurface inhomogeneities such as cracks and local stresses. For this purpose the specimen is magnetized to saturation in a high strength magnetic field at the beginning of any fretting fatigue experiment. After the magnetization and the removal of the magnetic field, a certain residual magnetism, known as the remanence, is left in the specimen. As the material of the specimens can be classified as magnetically hard, the behaviour of the specimens after magnetization to saturation is that of a permanent magnet.

As a consequence of the magnetoelastic interaction or, more briefly, magnetostriction, the distribution of the magnetization in the specimen is influenced by the fatigue load. The cyclic stress causes a change in the direction of the magnetization in the magnetic domains. The irreversible part of this change of magnetization leads to a gradually demagnitization of the magnetized specimen. The reversible part of change of magnetization, which is a result of cyclic rotation of the magnetization about its state of equilibrium, originates a flux change which induces a cyclic voltage in the pick-up coil. As a growing crack in the specimen causes a demagnetization and leads to a rapid decrease of the induction voltage, this voltage is utilized for the crack indication.

For the quantitative analysis of changes of the magnetic induction voltage curve the method of harmonic analysis was applied. The magnitudes and the phases of a definite number of harmonics were computed. The employed technique is the single frequency discrete Fourier analysis. Changes of the inductive voltage curve are detectable by comparison of spectra belonging to different numbers of load cycles /6/.

3. Experimental results and discussion

3.1 Fretting fatigue curves

Two series of fretting fatigue tests with the same material combination 34CrNiMo8 for the specimen and 100Cr6 for the pad but with different hardnesses were performed: The first consisted of soft specimens with a Vickers hardness of 480 HV for the specimen and 540 HV for the pad. The second series of tests consisted of a hard material combination with 840 HV for the specimen and 840 HV for the pad.

For the finite-life region of each S/N diagram a curve is plotted which fits the average of the experimental data. The underlaying equation for the linear regression calculation is of the type S=bNexpm, where N is the number of cycles, S is the alternating stress and b and m are constants related to the material and the experimental conditions. The assumed S/N relation can be estimated by fracture-mechanics considerations /7,8/.

3.1.1 Soft specimens, 480 HV

The results of the push-pull fretting fatigue tests on the soft specimens are shown as an overview in Fig.9 to Fig.12, together with a control curve obtained from push-pull tests without fretting on specimens with the same surface treatment. The results are presented for different surface treatments and normal forces of 50, 100 and 200 N for the polished specimens and normal forces of 50 and 100 N for the shaped specimens. Stresses are based on the minimum cross-sectional area of a specimen.

It will be noticed as a major difference between the fretting fatigue behaviour of the polished specimens and that of the shaped specimens that the relatively high dispersion of the test results is larger at the higher surface roughness of the shaped specimens. Thus it is difficult to detect a particularly marked influence of the two parameters surface roughness and normal force on the fretting fatigue behaviour from these overview figures. Therefore the stress amplitude, associated to a life time of 10exp6 cycles, versus normal force curves calculated from the relations of

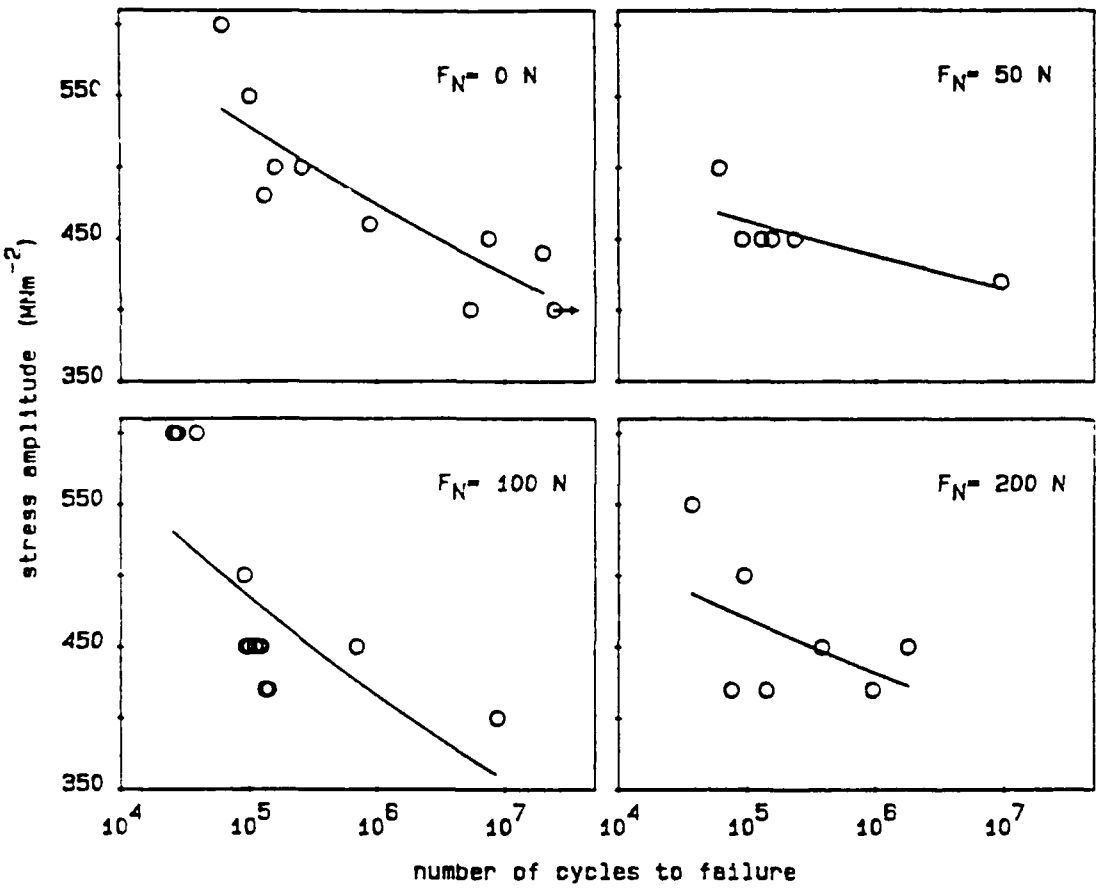

Specimen: 34CrNiMo6, tempered, 480 HV 0.4
polished parallel to sliding direction
roughness 0.45 µm CLA

Pad : 100Cr6, tempered, 540 HV 0.4
polished parallel to sliding direction
roughness 0.12 µm CLA

Fig.9 - Fatigue curve and fretting fatigue curves at normal forces of 50, 100 and 200 N of parallel polished specimens.
An arrow attached to a point, here and in the following S/N-diagrams, indicates that the specimen was unbroken at the end of the test.

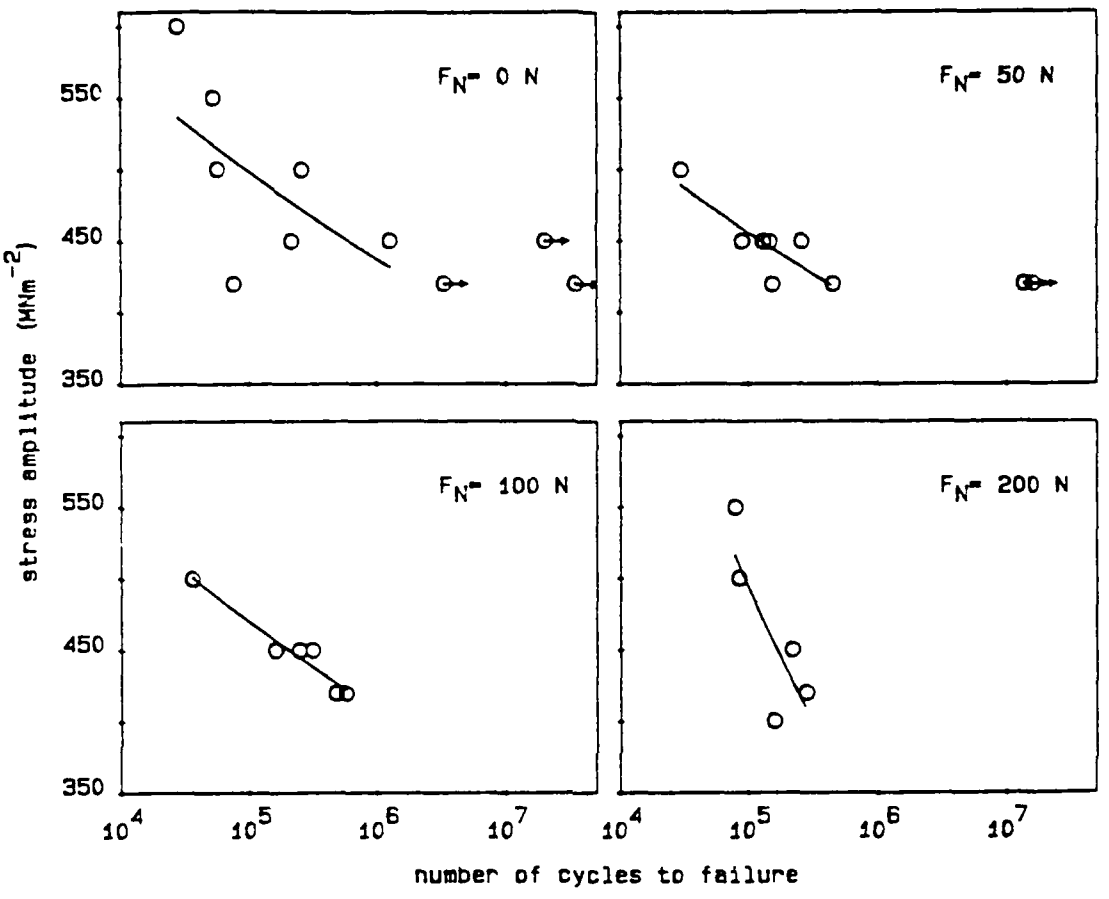

Specimen: 34CrNiMo6, tempered, 480 HV 0.4
polished perpendicular to sliding direction
roughness 0.32 µm CLA

Pad : 100Cr6, tempered, 540 HV 0.4
polished parallel to sliding direction
roughness 0.12 µm CLA

Fig.10 - Fatigue curve and fretting fatigue curves at normal forces of 50, 100 and 200 N of perpendicular polished specimens.

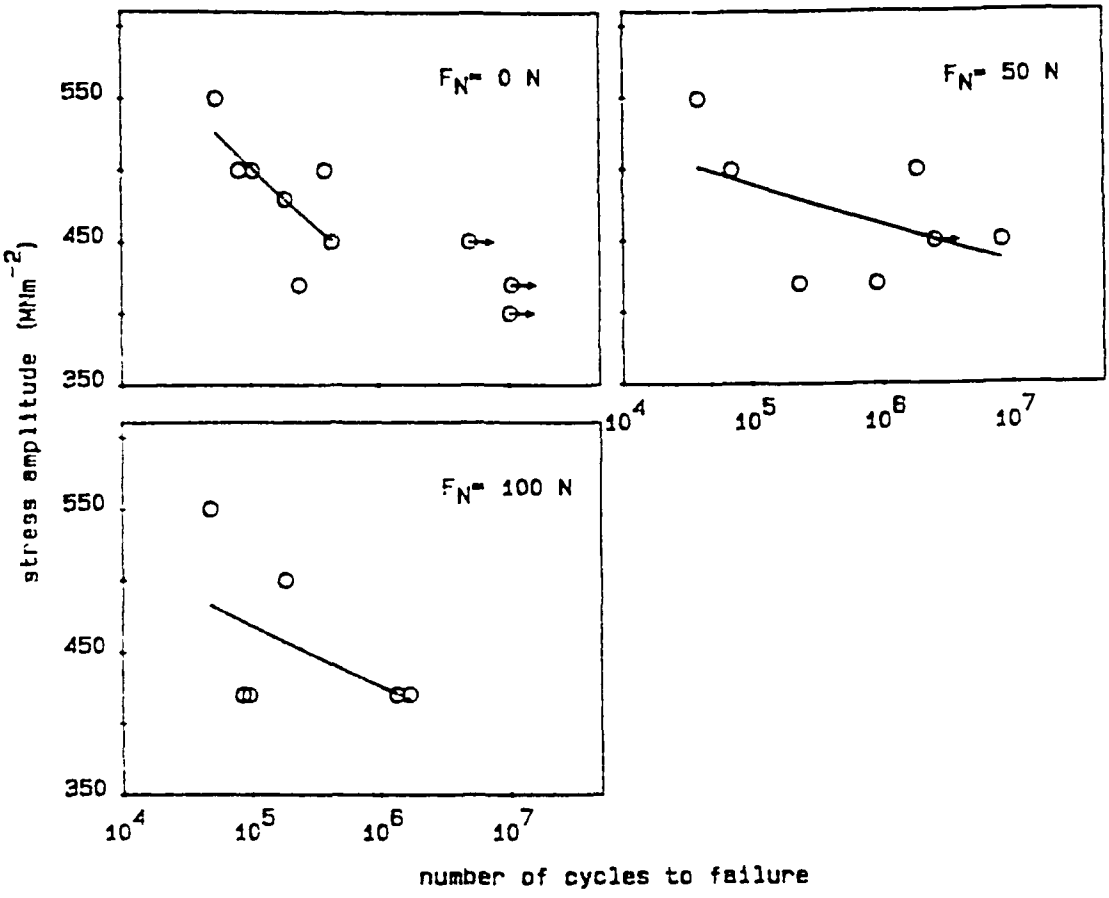

Specimen: 34CrNiMoB, tempered, 480 HV 0.4
shaped parallel to sliding direction
roughness 8.7 µm CLA

Pad : 100CrB, tempered, 540 HV 0.4
polished parallel to sliding direction
roughness 0.12 µm CLA

Fig.11 - Fatigue curve and fretting fatigue curves at normal forces of 50 and 100 N of parallel shaped specimens.

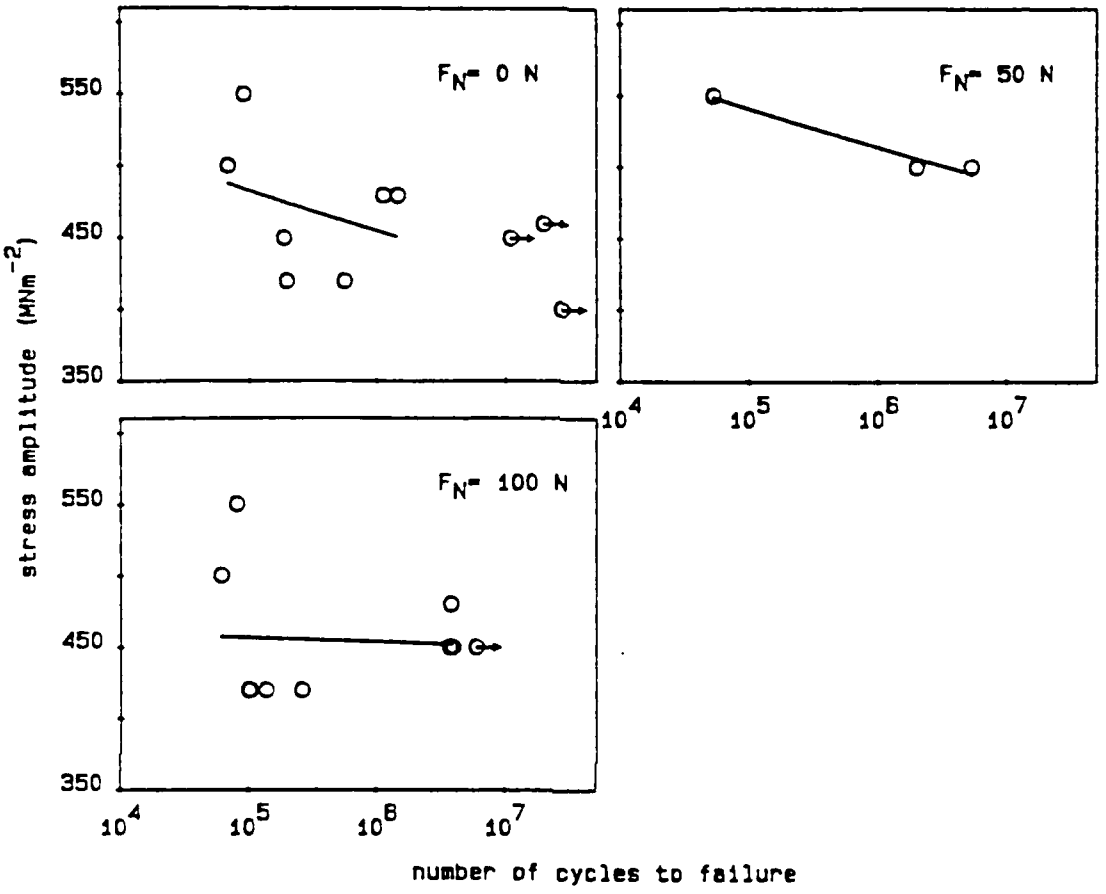

Specimen: 34CrNiMo6, tempered, 480 HV 0.4
shaped perpendicular to sliding direction
roughness 5.8 µm CLA

Pad : 100Cr6, tempered, 540 HV 0.4
polished parallel to sliding direction
roughness 0.12 µm CLA

Fig.12 - Fatigue curve and fretting fatigue curves at normal forces of 50 and 100 N of perpendicular shaped specimens.

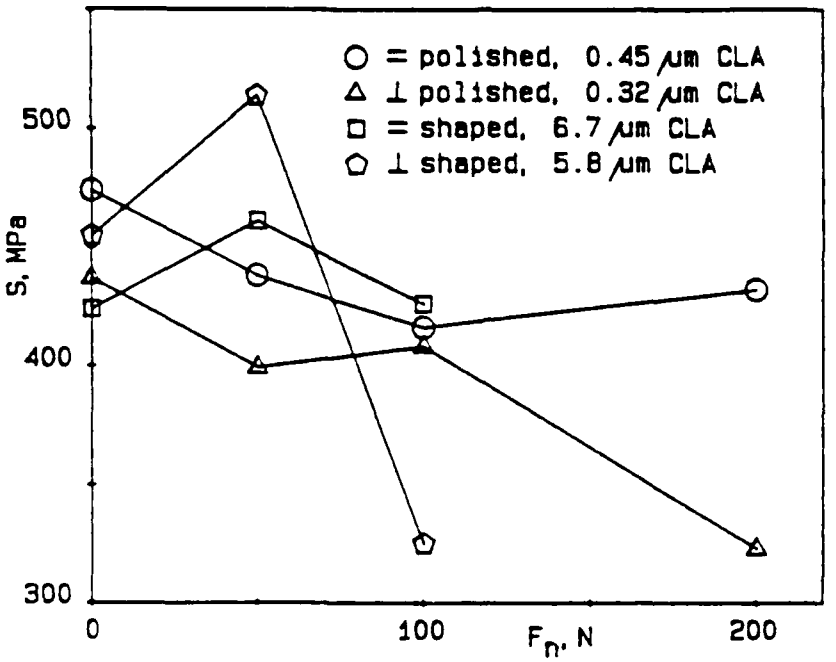

Life time: $N_B = 10^6$ cycles

F_n, N	S, MPa polished =	polished ⊥	shaped =	shaped ⊥
0	474	437	424	455
50	438	399	461	514
100	416	408	426	325
200	432	323		

Fig.13 - Relation between stress amplitude S, associated to a life time of 10exp6 cycles, and normal force Fn for different surface conditions. The table below contains the data calculated by the method of linear regression.

the average curves presented in the figures 9 to 12 are shown in Fig.13.

In the case of the polished specimens, the additional fretting produces a reduction in fatigue strength. The reduction of the perpendicular polished specimens is greater than that of the parallel to the sliding direction polished specimens. Attaching less importance to the fluctuations of the calculated data points it can be postulated, that the reduction of the fatigue strength increases with increasing normal force.

For the group of the shaped specimens a similar statement is not possible on account of the fluctuation. The disturbing influence of the rough surface, as a result of the notch effect of the groves, seems to dominate above the effect of the normal force.

3.1.2 Hard specimens, 840 HV

The results of fretting fatigue tests on hard specimens which were polished parallel and perpendicular to the sliding direction to a surface roughness of about 0.46 µm CLA are represented in Fig.14 and Fig.15 for different normal forces. For the normal force of 200 N only two points are present for the parallel and one point for the perpendicular polished specimens.

The dispersion of the data points is not as great as that of the soft specimens. The two overview figures illustrate that there is a definite effect due to fretting on the fatigue lives of both the parallel and the perpendicular polished specimens. This effect manifests itself in the form of reduced lives at corresponding stress levels. The two control curves of pure fatigue show no significant difference between the two directions of polishing, that means, the direction of polishing of this surface treatment has no particular influence on the fatigue behaviour. The difference of life times is due to the additional fretting effect, which is influenced by the direction of polishing. These effects are more clearly detectable in a representation of the life time at a definite stress level of 600 MPa, which is near the fatigue limit. This interrelationship is shown in Fig.16, where the life time axis is log-scaled. The data

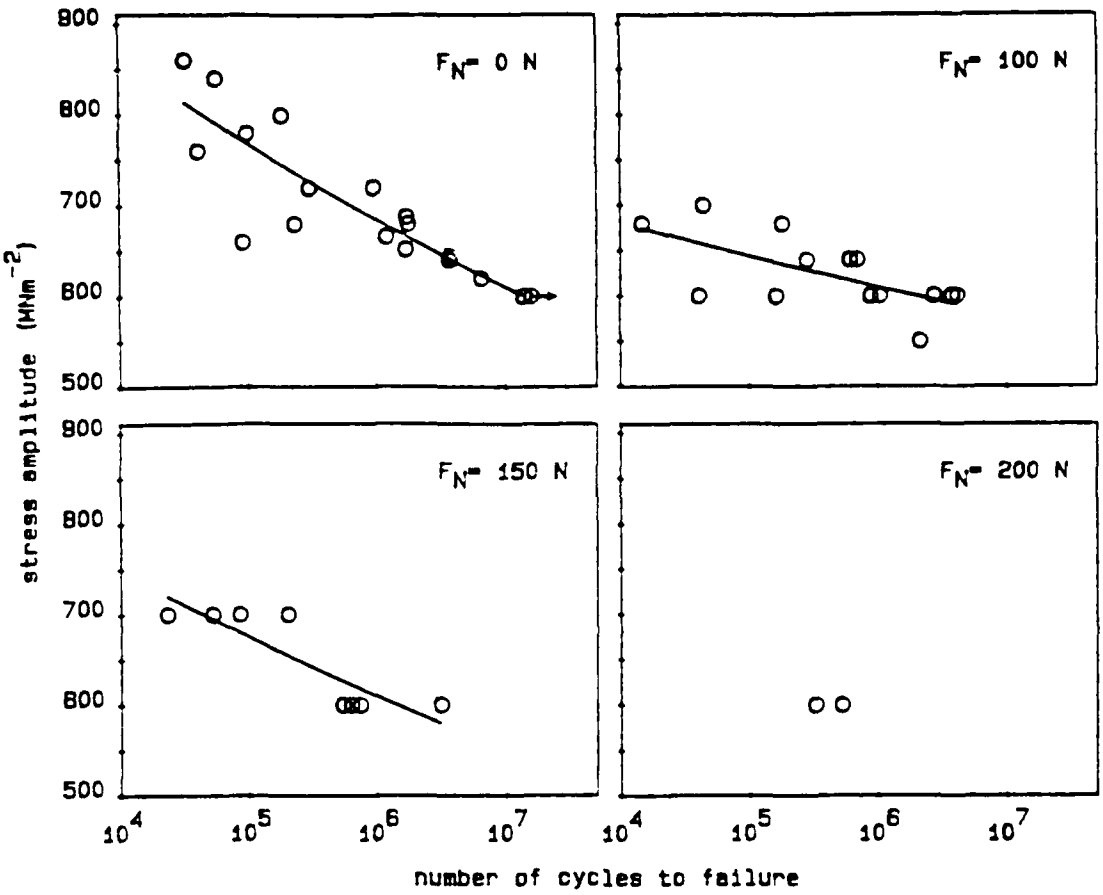

Specimen: 34CrNiMo8, tempered, 850 HV 0.4
polished parallel to sliding direction
roughness 0.5 µm CLA

Pad : 100Cr6, tempered, 840 HV 0.4
polished parallel to sliding direction
roughness 0.12 µm CLA

Fig.14 - Fatigue curve and fretting fatigue curves at normal forces of 100, 150 and 200 N of parallel polished specimens.

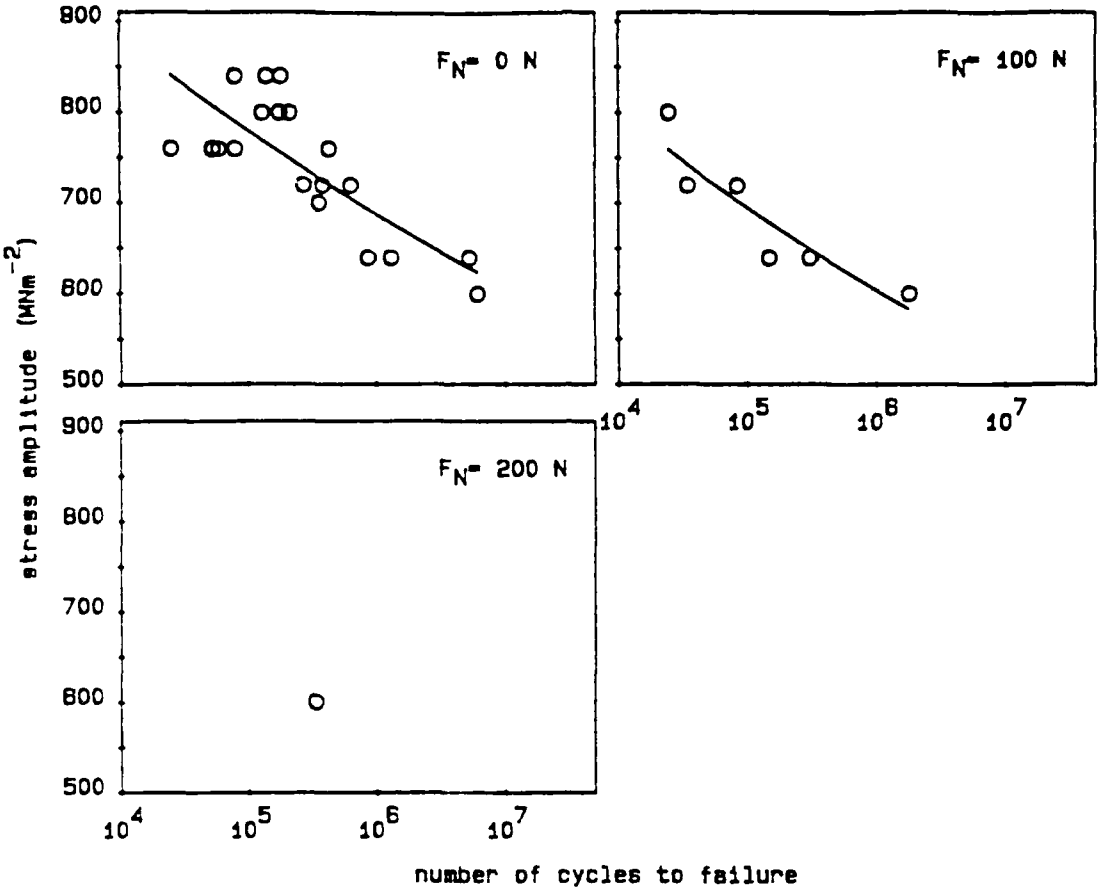

Specimen: 34CrNiMo6, tempered, 840 HV 0.4
polished perpendicular to sliding direction
roughness 0.42 µm CLA

Pad : 100Cr6, tempered, 840 HV 0.4
polished parallel to sliding direction
roughness 0.12 µm CLA

Fig.15 - Fatigue curve and fretting fatigue curves at normal forces of 100 and 200 N of perpendicular polished specimens.

points were calculated from the average curves drawn in Fig.14/15.

The life time belonging to the stress level of 600 MPa of the parallel polished specimens is greater than the life time of the perpendicular polished specimens for all considered normal forces. The differences are 11% at pure fatigue, 73% at 100 N normal force and 33% at 200 N normal force related to the perpendicular polished specimens.

The life time of the fretted specimens related to the life time of the normal fatigue specimens is for the parallel polished specimens 14% at 100 N, 10% at 150 N and 3% at 200 N normal force and for the perpendicular polished specimens 9% at 100 N and 2.7% at 200 N normal force.

It will be noticed that the influence of the direction of polishing seems to be maximal at the normal force region of 100 N and that it is lower at 200 N normal force. It is supposed that the decrease of the surface influence at normal forces near 200 N and greater is due to the decreasing slip amplitude, which results from the finite rigidity of the fretting apparatus, so that the damaging fretting effect is reduced above a definite normal force with increasing normal force. Owing to the loss of slip amplitude caused by the deformable fretting device the effect of fretting may be maximal at a definite normal force.

3.2. Light microscopy examinations

Fig.17 shows the crack surfaces of three representative ~80 HV specimens, which were polished perpendicular to the sliding direction, after fretting fatigue under 50, 100 and 200 N normal force and 450 MPa fatigue load. Typically for the fretting fatigue phenomenon is that all specimens failed near the edge of the fretting mark and that the crack originates always at the fretted surface, which is on the bottom of each picture. The contact region is marked by a dark edge caused by fretting debris. The appearance of the crack surfaces is that of a typical fatigue fracture where two distinct regions can be distinguished. The first is a relative smooth area, through

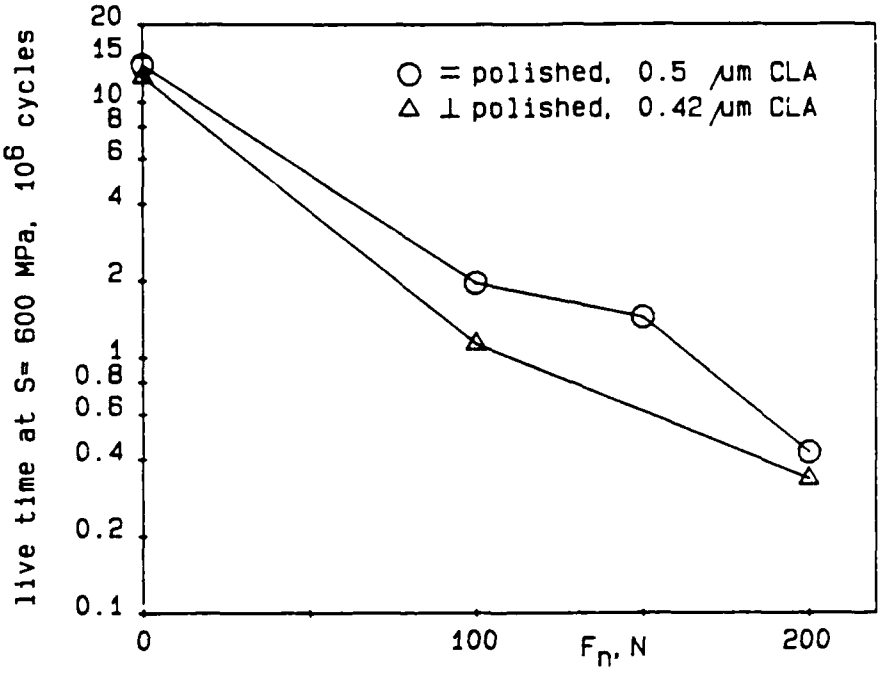

Stress S=600MPa

F_n, N	N_B, 10^6 cycles polished =	⊥
0	13.9	12.5
100	1.9	1.1
150	1.4	-
200	0.4	0.3

Fig.16 - Relation between live time Nb, associated to a stress amplitude of S= 600 MPa, and normal force Fn for two directions of polishing. The table below contains the data calculated by the method of linear regression.

which the fatigue crack has spread slowly, starting from the fretting mark on the bottom. The remainder of the fracture surface shows a typical rough fracture where the failure has been catastrophic.

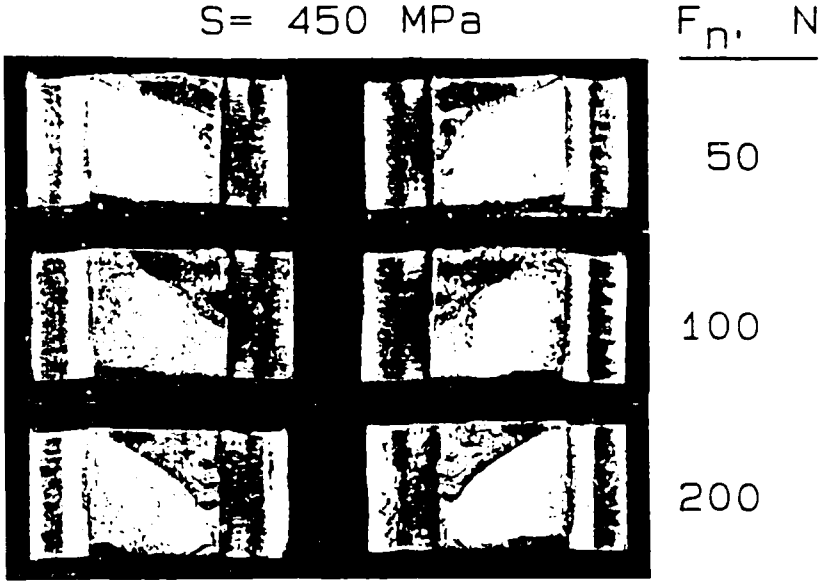

Fig.17 - Series of photographs of the crack surfaces of perpendicular polished 480 HV specimens fretted under different normal forces at a fatigue load of 450 MPa.

Fig.18 shows an overview of the locations of breaks of polished and shaped 480 HV specimens, composed of four pieces. Three specimens of each piece from left were unfretted specimens without fretting scars. It is remakable that the crack of the perpendicular polished and shaped specimens more often ends outside of the fretting mark. It can be deduced from the analysis of the crack surface that in these cases the crack starts beneath the surface under the fretting mark and progresses angular to the surface which is cut outside the fretting mark.

Fig.19 shows in the left picture a growing fretting fatigue initiated crack within the fretting mark

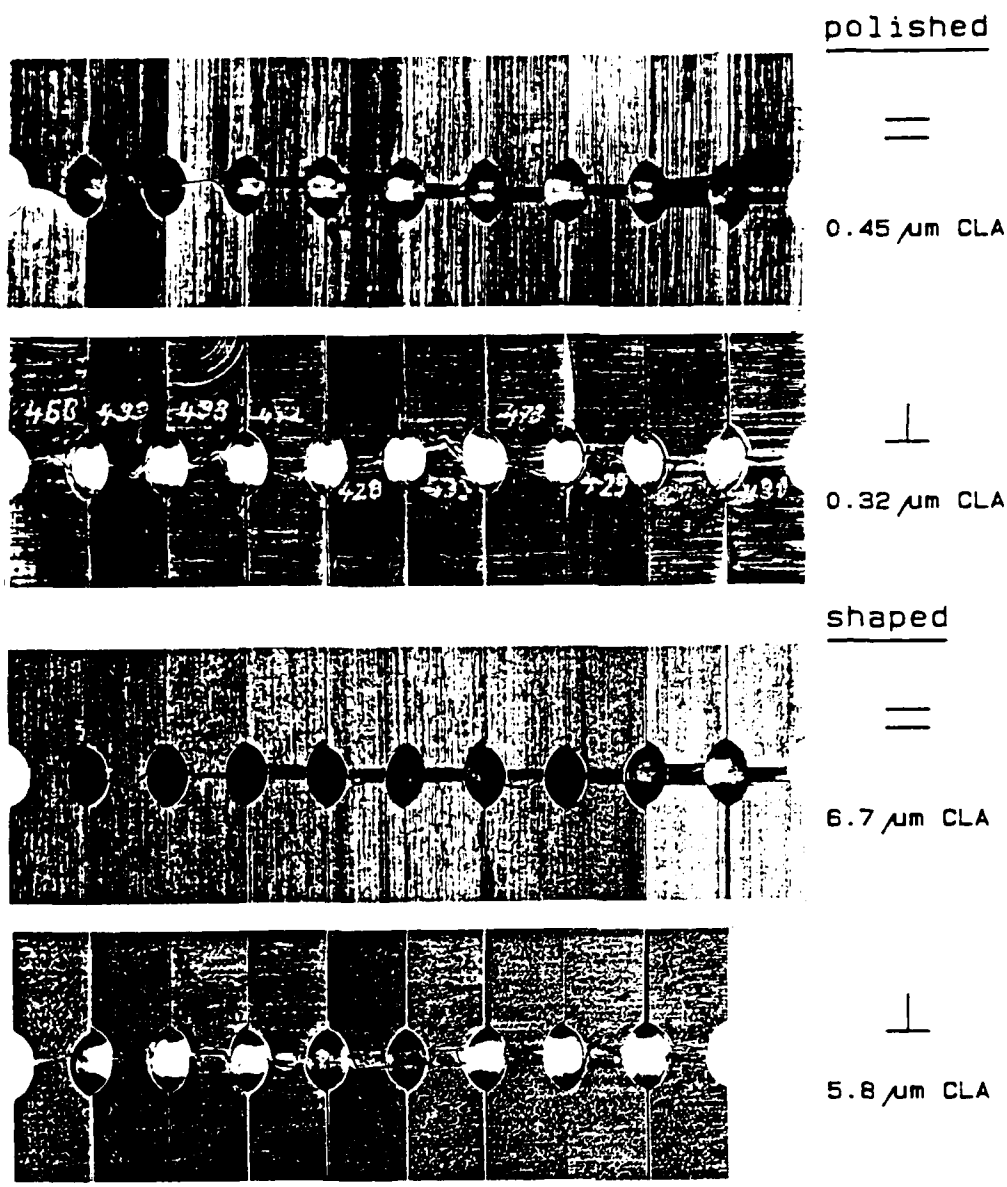

Fig.18 - Break configuration of polished and shaped 480 HV specimens.

and in the right picture the final crack 10000 loading cycles later. For the left snapshot the fretting fatigue loading was stopped after the detection of the crack by the magnetic induction method and the specimen was removed from the loading apparatus. After the photography has been made, the specimen was inserted to the loading device again and further loaded as long as the crack needed to progress through the whole cross section. As the maximum frictional stresses on the fretting surface are repeated at the edges of the contact region the crack is generated near this area: near the upper left corner of the fretting mark.

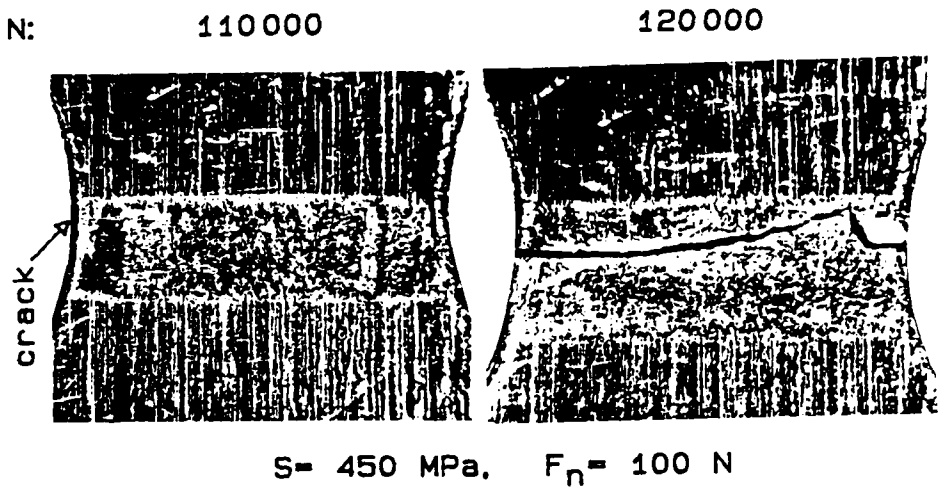

Fig.19 - Development of a fretting fatigue crack within the fretting scar of a parallel to the sliding direction polished 480 HV specimen. Roughness 0.42 µm CLA, specimen number 415.

Fig.20 shows a fretting fatigue initiated crack within the fretting mark of a perpendicular polished specimen (upper picture). The lower picture shows the backside of the specimen. The crack, which has started within the fretting mark, similar to the behaviour of the parallel polished specimens, has not approached the region near the backside's surface, so that the backside shows not yet marks of deformation. The crack was detected by the magnetic induction method.

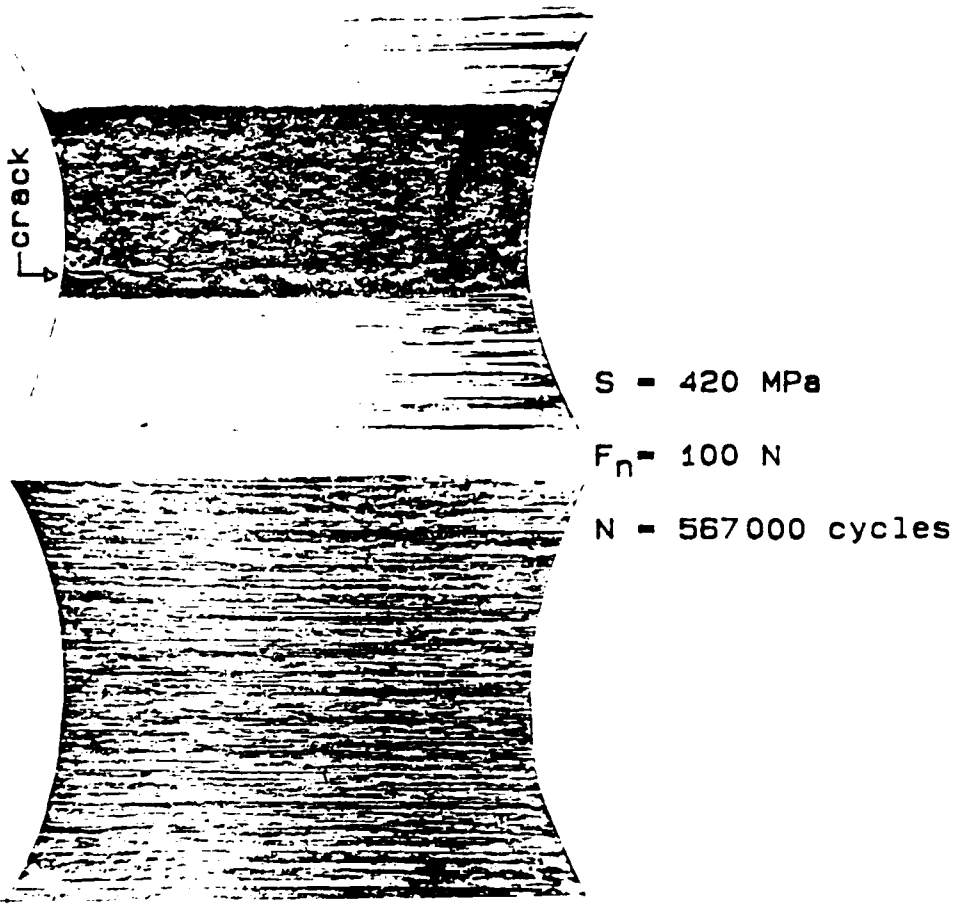

Fig.20 - Fretting fatigue initiated crack within the fretting mark of a perpendicular to the sliding direction polished 480 HV specimen. Roughness 0.25 µm CLA, specimen number 464.

An example of a surface crack outside of the fretting region, which was sometimes observed preferentially at perpendicular polished and shaped specimens, is shown in Fig.21. The unfretted backside of the specimen, which is represented in the lower picture, shows the trace of the crack which has passed through the full thickness of the specimen under the fretting mark. As the crack on the unfretted side

shows clear deformations, it is supposed, that the crack was generated beneath the surface in a small distance from the contact area and propagates angular to the surface.

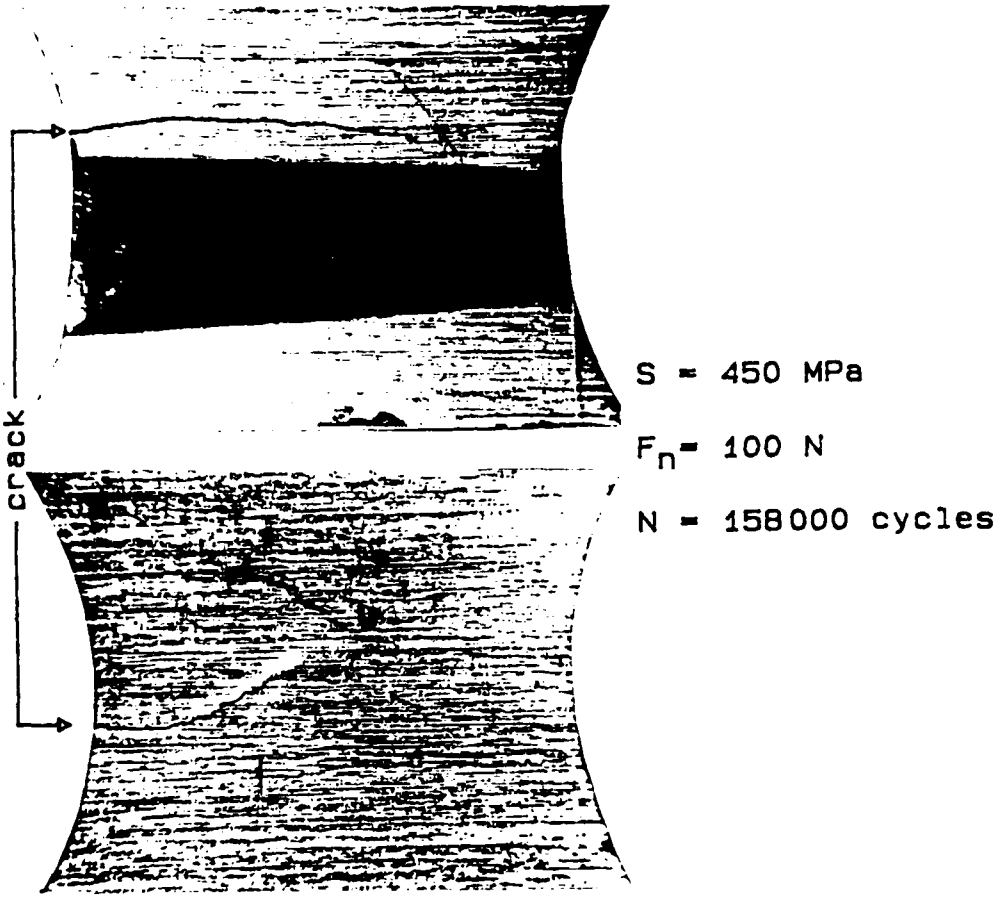

Fig.21 - Crack in a perpendicular polished specimen which cuts the surface beside the fretting scar. Roughness 0.34 µm CLA, specimen number 393.

Fig.22 illustrates a characteristic fretting fatigue crack in a hard perpendicular polished 840 HV specimen at N= 35000 cycles. The crack of a length of 1.4 mm has propagated perpendicular to the fretting direction, i.e. the sliding direction, which is in

the direction of the alternating stress. The crack is located a short distance of 0.2 mm inside the edge of the contact region. The whole length of the contact region parallel to the sliding direction is 1.2 mm. At the crack edges near the tip of the crack, clear marks of adhesive wear are visible.

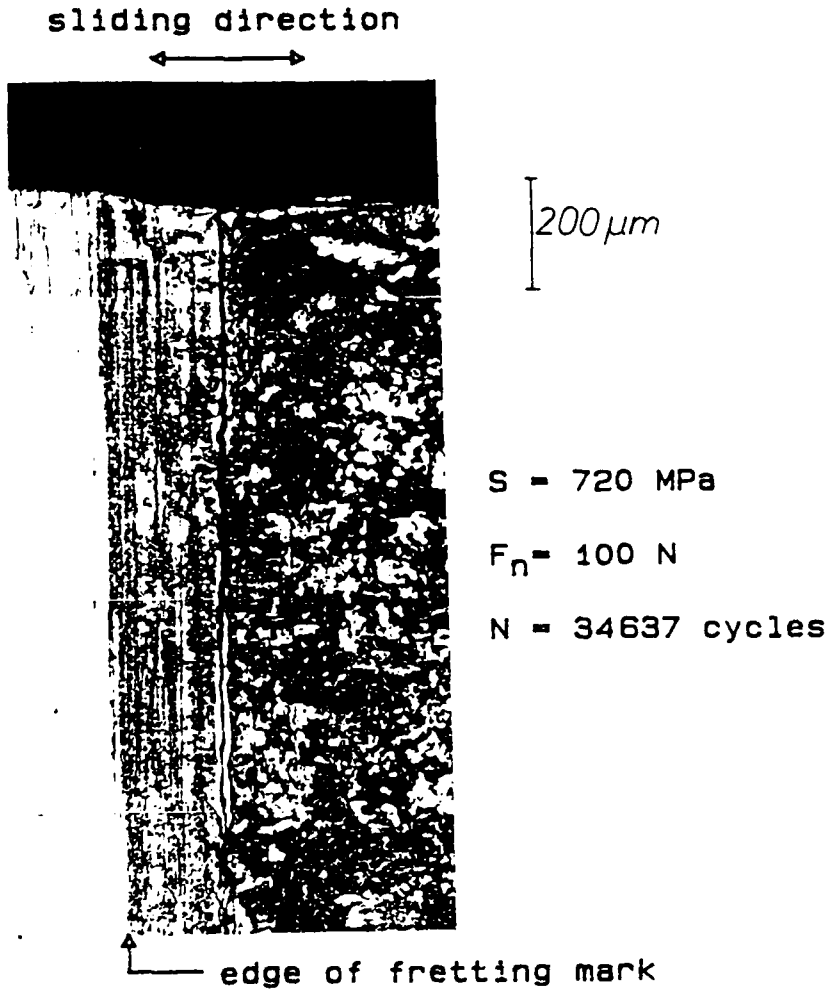

Fig.22 - Section of the fretting scar showing the development of a fretting fatigue crack. Perpendicular polished 840 HV specimen No. 461, Roughness 0.42 µm CLA.

3.3 Friction and wear

Friction and wear are manifestations of the same tribological event, i.e. formation of microcontacts or real area of contact. The friction force is a macroscopic measurement of the summation of the local resistances to motion at individual contacts. Simi-

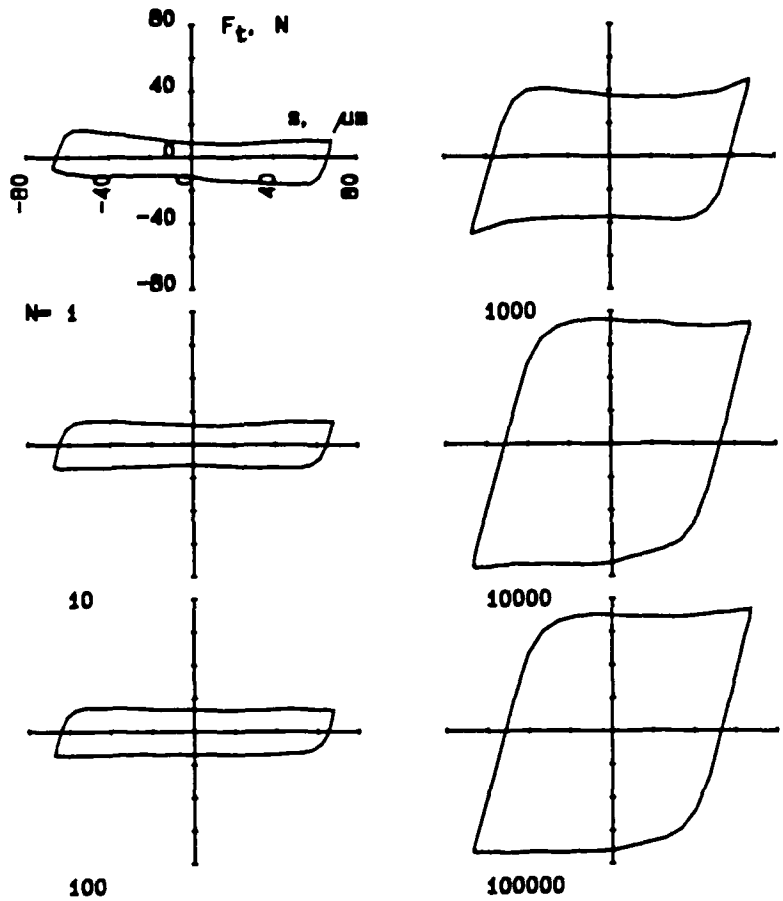

S= 450 MPa, F_n= 100 N, N_b= 120000 cycles

Fig.23 - Series of friction force-displacement hysteresis loops gathered during the life time of a parallel polished 480 HV specimen. Specimen number 415.

larly, wear is a macroscopic measurement of microscopic events.

3.3.1 Friction force - displacement hysteresis

A series of complete friction force-displacement hysteresis loops, gathered during the life time of a parallel polished 480 HV specimen is presented in Fig.23. The behaviour is characterized by two regimes. At low cycles the friction force increases initially and then reaches an approximate constant value at higher cycles. The slip amplitude decreases from s= 65 μm at the beginning of the test to s= 52 μm at the end with increasing friction force caused by the elastic deformation of the fretting device.

Fig.24 shows the hysteresis loops of a perpendicular polished 480 HV specimen under the same loading conditions. The behaviour is again characterized by two regimes, but these are different from those shown in Fig.23. The initial behaviour during the first ten cycles is nearly the same, but then the tangential force raises more rapidly so that the steady-state behaviour is reached at a lower number of loading cycles. The steady-state friction force of the perpendicular polished specimen is lower than that in the case of the parallel polished specimen. The last loop, which is gathered a few cycles before cracking, shows a distinct asymmetry caused by an existing crack.

Similar to the magnetic method, this asymmetry, which always appears when a crack changes the deformation behaviour of the specimen as well as the friction force when the fretting pad passes the surface crack, can also be used as a sensitive indicator for cracks.

Figures 25-26 show the friction hysteresis loops for shaped 480 HV specimens. In contrast to the polished specimens a rapid increase of the friction force during the first 10 cycles is observed. Even a distinct increase during the first half loading cycle is visible, which leads to an asymmetric first loop.

The starting point of the data aquisition lies on the negative friction force axis and the hysteresis loop is passed clockwise.

The qualitative behaviour of the parallel and perpendicular shaped specimens is nearly the same.

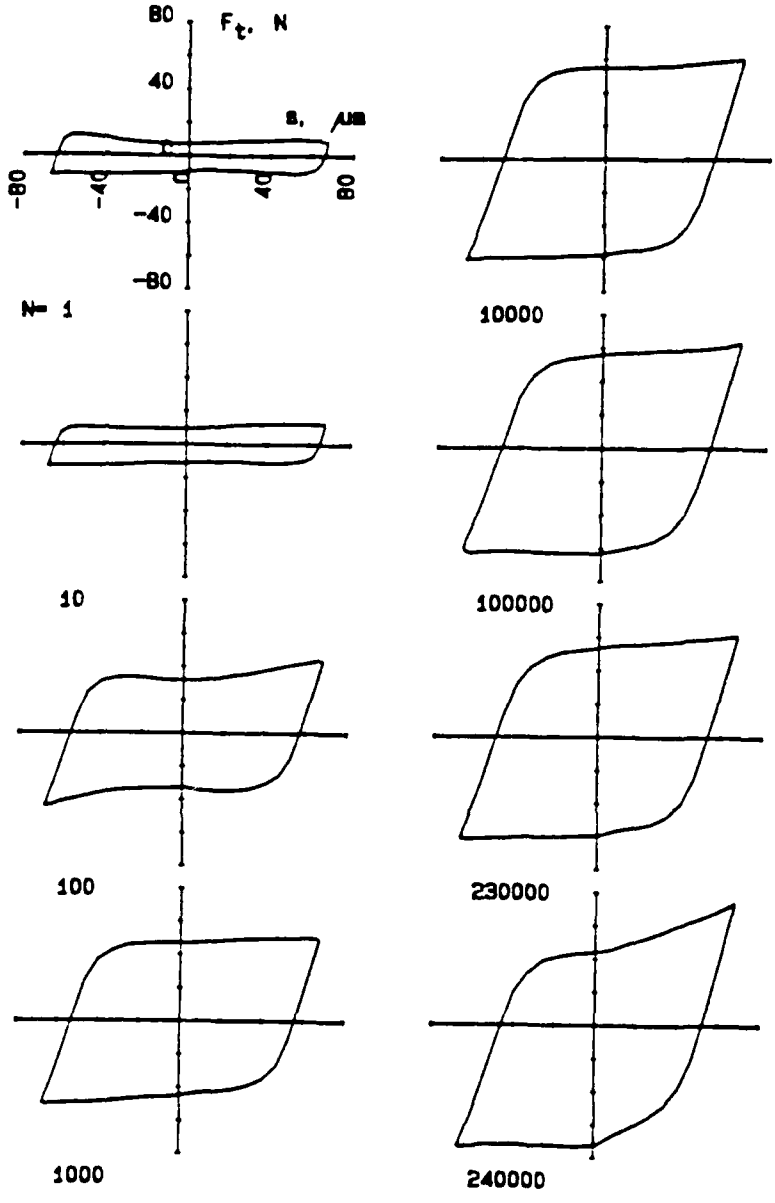

Fig.24 - Series of friction force-displacement hysteresis loops gathered during the life time of a perpendicular polished 480 HV specimen. Specimen number 430.

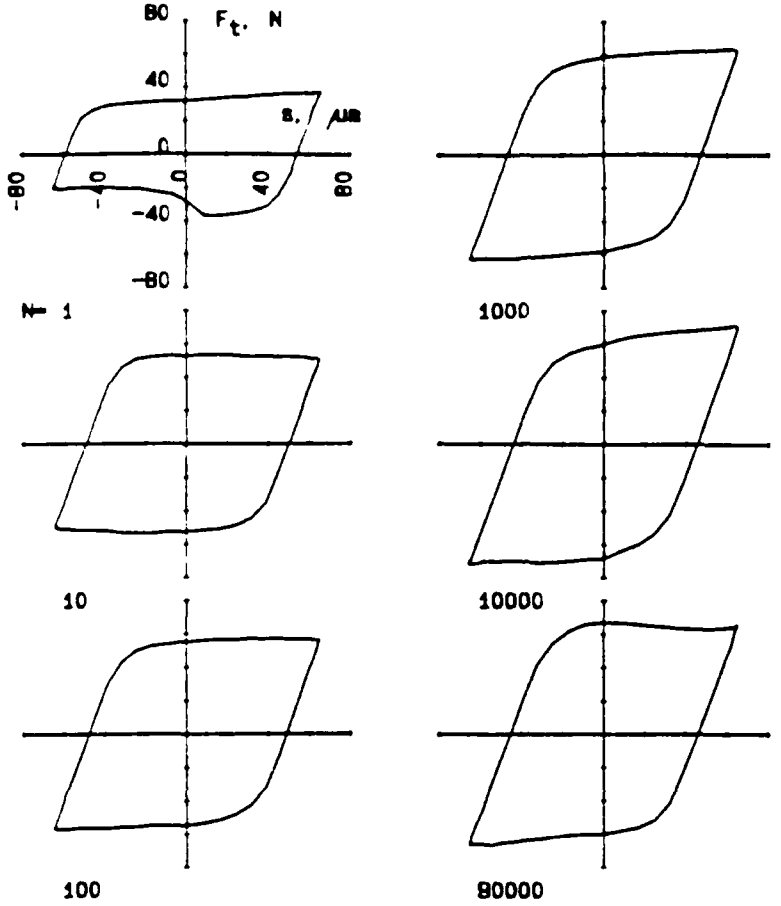

S= 420 MPa, F_n= 100 N, N_D= 85174 cycles

Fig.25 - Series of friction force-displacement hysteresis loops gathered during the life time of a parallel shaped 480 HV specimen. Specimen number 512.

Compared with the polished specimens, the initial friction force of the shaped specimens during the first cycle is essentially greater but there is only a slight difference during the first quarter cycle. At steady state the friction force is nearly the same for polished and shaped specimens.

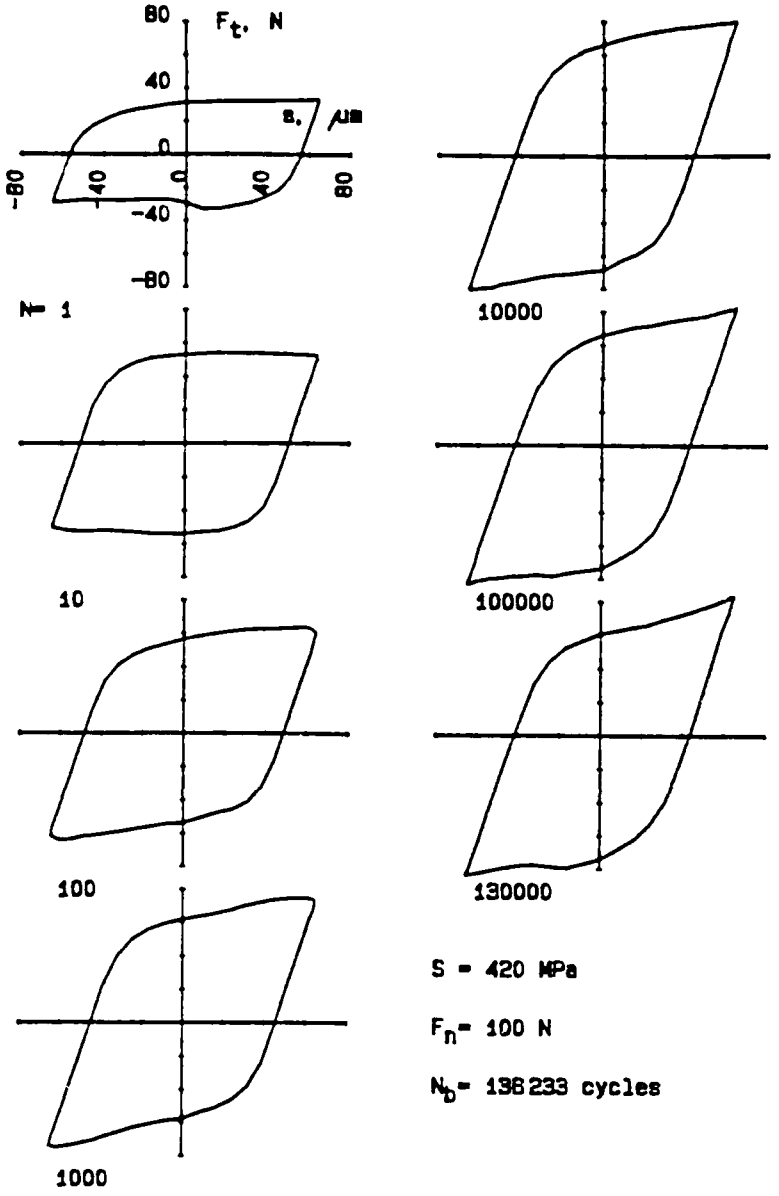

Fig.26 - Series of friction force-displacement hysteresis loops gathered during the life time of a perpendicular shaped 480 HV specimen. Specimen number 521.

3.3.2 Friction coefficient

Intermittently throughout an experiment the friction force-displacement hysteresis loop was re-recorded. The coefficient of friction was then calculated from the ratio of the maximum rate of friction force and the constant normal force during one load cycle.

For increased clarity, friction measurements are plotted versus log(number of cycles) rather than versus a linear time scale.

Fig.27 shows the relationship of polished and shaped specimens corresponding to the behaviour of the friction force-displacement hysteresis loops which are represented in Fig.23-26. The alternating fatigue load and therefore the slip amplitude is different for the two types of surface treatment.

As already indicated in Fig.23/24, the friction behaviour of the two types of polished specimens is

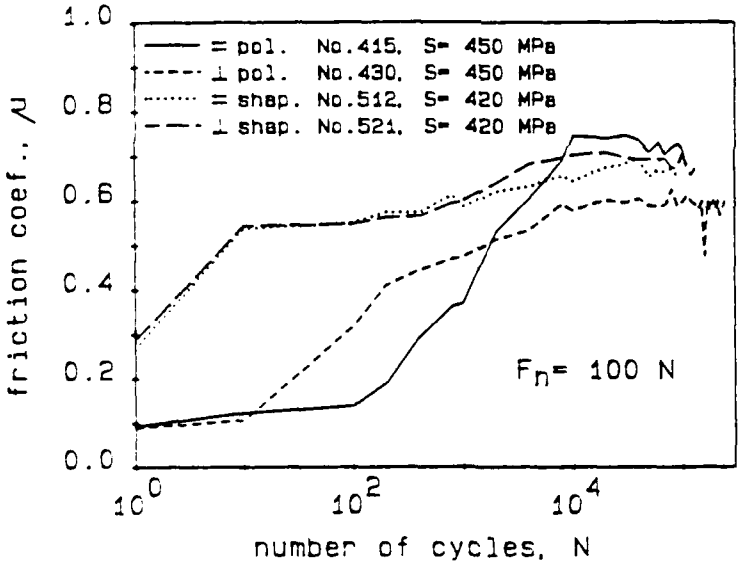

Fig.27 - Coefficient of friction vs. number of cycles of parallel and perpendicular polished and shaped specimens. The relations correspond to those of the figures 23 to 26.

quite different. For lower numbers of cycles the friction coefficient of the parallel polished specimen is lower than that of the perpendicular polished specimens. After the crossover at 2000 cycles the situation is reversed. The higher friction force, which is active during the main part of the life time, induces a higher alternating shear stress in the surface region which facilitates crack initiation. The result is: the life time of the parallel polished specimen is shorter compared to that of the perpendicular polished specimen.

The shaped specimens show no significant difference in their friction behaviour in relation to the direction of shaping. The result is: both shaped specimens have nearly the same life time.

Comparing the curve of the parallel polished specimen with those of the shaped specimens, it is noticed, that the friction coefficient in the steady state region is nearly equal. The live time of the polished specimen ends in the small intervall of cycles which is built by the ends of live time of shaped specimens. It is supposed, that this short life time of the specimen with the better surface is caused by the higher friction force in addition to the higher fatigue load.

Figures 28 - 29 show the relationship between the coefficient of friction and the number of cycles for polished and shaped 480 HV specimens at different surface and fatigue loading conditions at an equal normal force of 100 N. Each surface and loading parameter set is represented by three representative curves. The behaviour of the polished specimens is characterized by the three regimes which was already deduced from the friction force-displacement hysteresis of the figures 23 - 24. At the first 200 cycles the coefficient of friction rises slowly followed by a rapid increase to the friction coefficient at steady state which is taken to be the value after 10000 cycles. The essential difference of the friction behaviour of the shaped specimens is the immediate increase of the coefficient of friction from the beginning of the first cycle over the whole fretting duration. The initial friction coefficient of the polished specimens is about 0.1 whereas in the case of the shaped specimens it is about 0.3. The

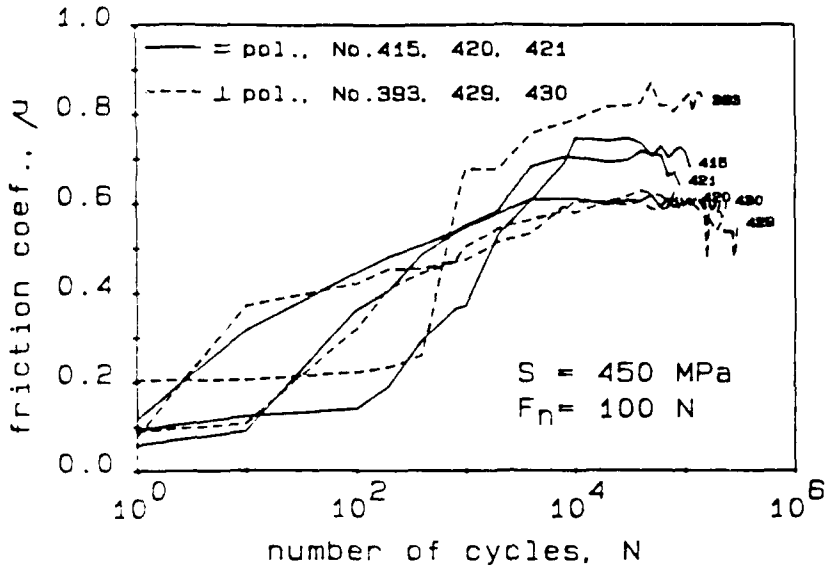

Fig.28 - Coefficient of friction vs. number of cycles of parallel and perpendicular polished 480 HV specimens.

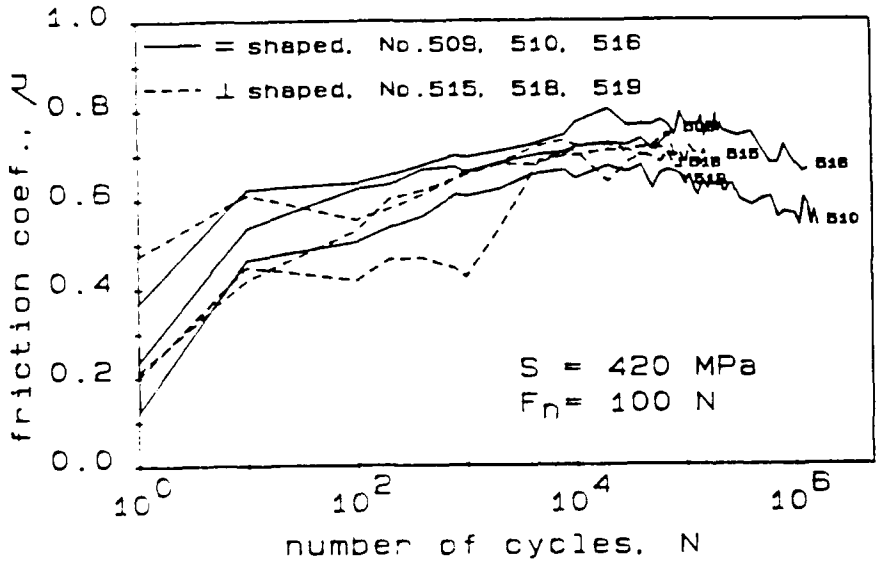

Fig.29 - Coefficient of friction vs. number of cycles of parallel and perpendicular shaped 480 HV specimens.

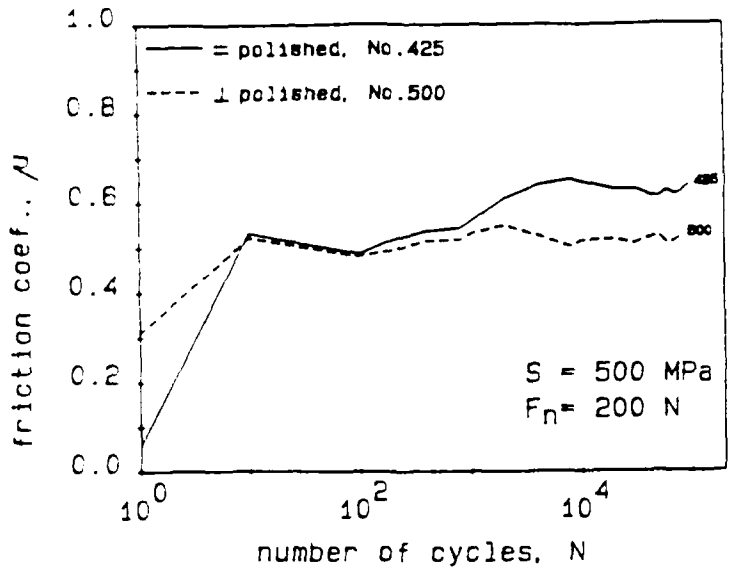

Fig.30 - Coefficient of friction vs. number of cycles of a parallel and a perpendicular polished 480 HV specimen.

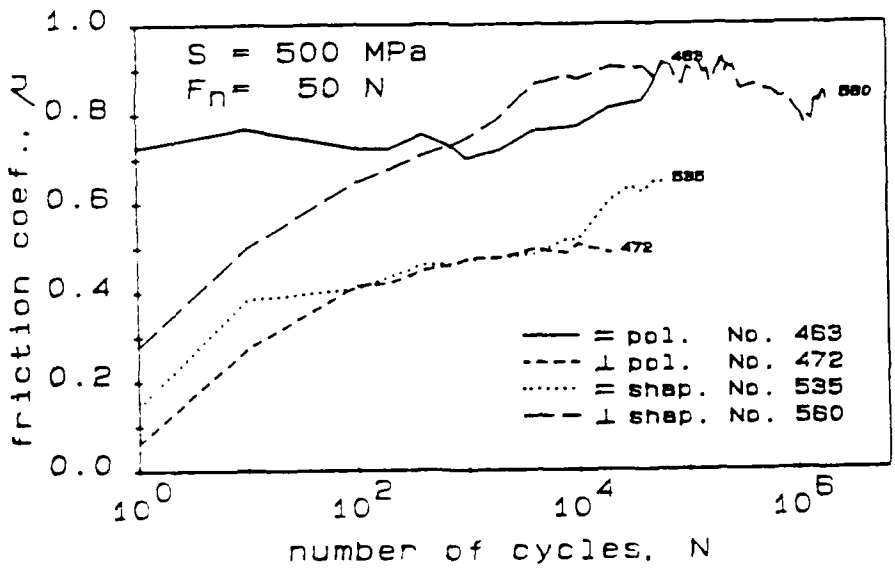

Fig.31 - Coefficient of friction vs. number of cycles of parallel and perpendicular polished and shaped 480 HV specimens.

friction coefficient at steady state has in both cases nearly the same value 0.65.

Figures 30-31 represent the friction behaviour of 480 HV specimens at high and low normal forces. Polished specimens at a normal force of 200 N show a rapid increase of the friction coefficient during the first 10 cycles followed by a lower increase during the whole test duration. The friction coefficient at steady state achieves the value of 0.6 for the parallel polished specimen and the value of 0.5 for the perpendicular polished specimen.

The friction behaviour of polished and shaped specimens at 50 N normal force is shown in Fig.31. It is remarcable that a high steady state friction coefficient of 0.85 is achieved in the cases of parallel polished and perpendicular shaped specimens. In spite of the high friction the perpendicular shaped specimens have had a relatively long life time.

3.3.3 Frictional energy dissipation

Slip of the contact surfaces against finite friction gives a frictional energy dissipation because a force is applied over a distance (even though it is a short distance). This energy which is caused by plastic deformation effects and is dissipated in a complete loading cycle may be represented graphically as the area of the friction force-displacement hysteresis loop. The area within the loop represents an energy dissipation:

$$\Delta E = \oint F_t \, ds$$

With the low measuring frequency of 1 Hz, the isothermal curve is closely followed. The total energy dissipated is large at high speeds (many stress cycles per second). This energy loss shows up as heat.

Figures 32-33 show the energy dissipation per cycle as a function of the number of loading cycles in a log-scale representation of 480 HV specimens at different surface and loading conditions. The results derive from the friction force-displacement hysteresis loops and correspond to the figures 23-27. The values of the dissipated energy are calculated for the beginning of each decade for the intervall of cycles 1 to 10000, then 10 values are calculated per

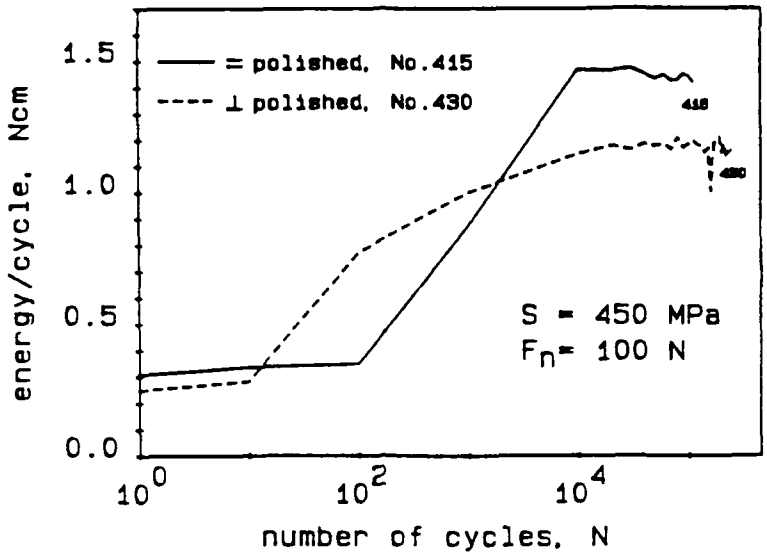

Fig.32 - Dissipated energy per cycle versus number of loading cycles of parallel and perpendicular polished 480 HV specimens.

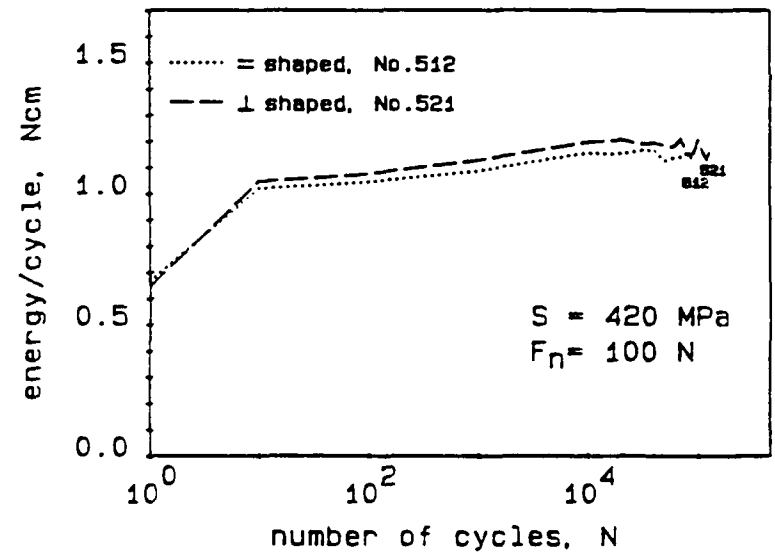

Fig.33 - Dissipated energy per cycle versus number of loading cycles of parallel and perpendicular shaped 480 HV specimens.

decade.

The graph of the dissipation energy is similar to that of the friction coefficient (Fig.27). The curves reflect the same friction behaviour because the shape of the friction force-displacement hysteresis loops is nearly trapezoidal and the dependence of slip amplitude from friction force is relatively weak.

3.3.4 Linear wear rate

The figures 34-38 show the results for linear wear versus number of cycles of 480 HV specimens of different surface treatments under various loading conditions. The plotted linear wear is the summation, for both specimen and pad, of the change in dimensions perpendicular to the original datum surface including the possibly amount of trapped fretting debris.

The wear characteristics of 8 specimens at a cyclic stress of 420 MPa and a normal force of 100 N, always two with the same surface treatment, are shown

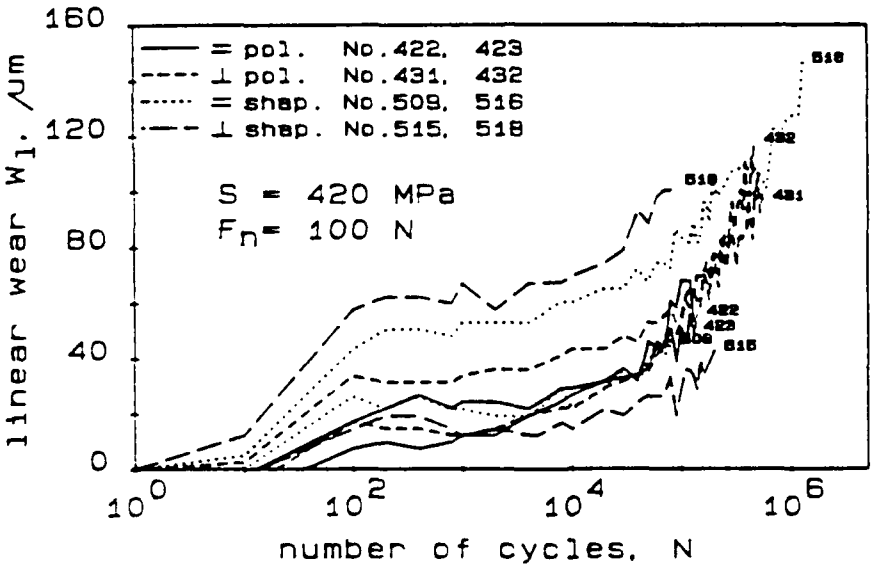

Fig.34 - Total linear wear vs. number of cycles of parallel and perpendicular polished and shaped 480 HV specimens.

in Fig.34. The stress level is near the endurance limit of unfretted specimens. The shape of all curves is nearly the same. The difference in the amount of linear wear is caused mainly by the different wear behaviour during the first 10 to 100 cycles. This is most probably caused by the mismatch of the traces on wear scars of pad and specimen which also leads to a large variation of the wear results.

Fig.35 shows the comparison of parallel and perpendicular polished specimens at a fatigue load of 420 MPa and normal forces of 50, 100 and 200 N. It is noticed that the wear rate is relatively low at 200 N normal force. This is caused by the dependence of the slip amplitude from normal force. The wear rate falls to zero at both small and large normal forces. At small normal forces there is extensive slip but the clamping pressure and hence the frictional shear stresses are small. At large values of the normal force, the large clamping pressure reduces the size of the slip region and the amplitude of slip and hence the wear rate to negligible proportions.

The wear behaviour of a parallel and a perpendicular shaped specimen at a normal force of 100 N and of a parallel shaped specimen at 50 N normal force, which has no pendant at the same fatigue load, is shown in Fig.36. Comparing the results with those of Fig.35 it can be noticed, that the initial increase of linear wear during the first hundred cycles of the shaped rough specimens is steeper than in the case of the smooth polished specimens.

The wear behaviour of polished and shaped 480 HV specimens at large slip amplitudes, due to a fatigue load of 500 MPa at 100 N normal force, is presented in Fig.37. The polished specimens show nearly the same behaviour with a low wear rate compared with that of the shaped specimens, which show a different behaviour related to the shaping direction. The perpendicular shaped specimen has the higher wear rate whereas the parallel shaped has the lower.

At the end of each fretting fatigue test the final linear wear of the pad alone was estimated from measurement of the wear scar diameter and from the determination of weight loss of the pad. The final linear wear of the specimen is then nearly equal to the difference between the total wear and the wear

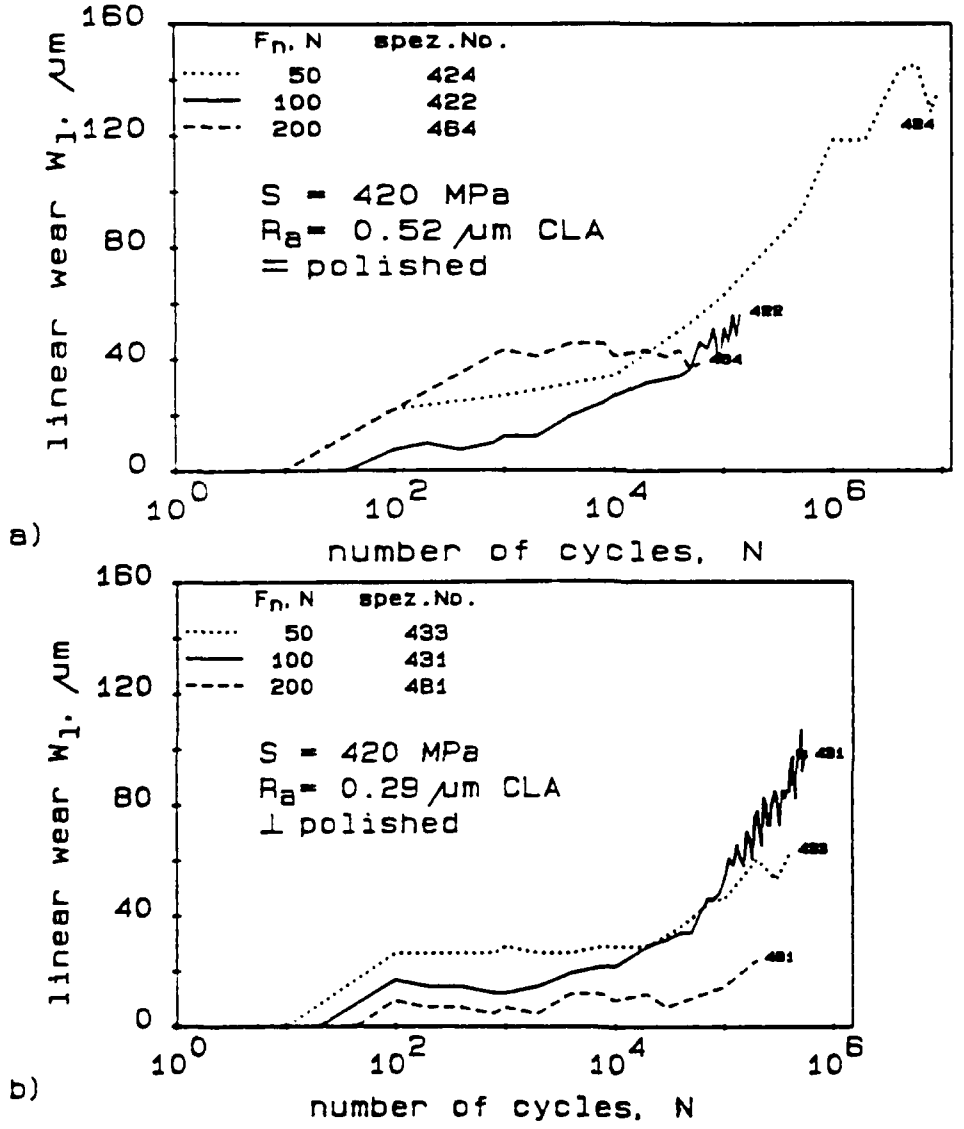

Fig.35 - Total linear wear vs. number of cycles of polished 480 HV specimens at normal forces of 50, 100 and 200 N.
a) parallel polished, b) perpendicular polished.

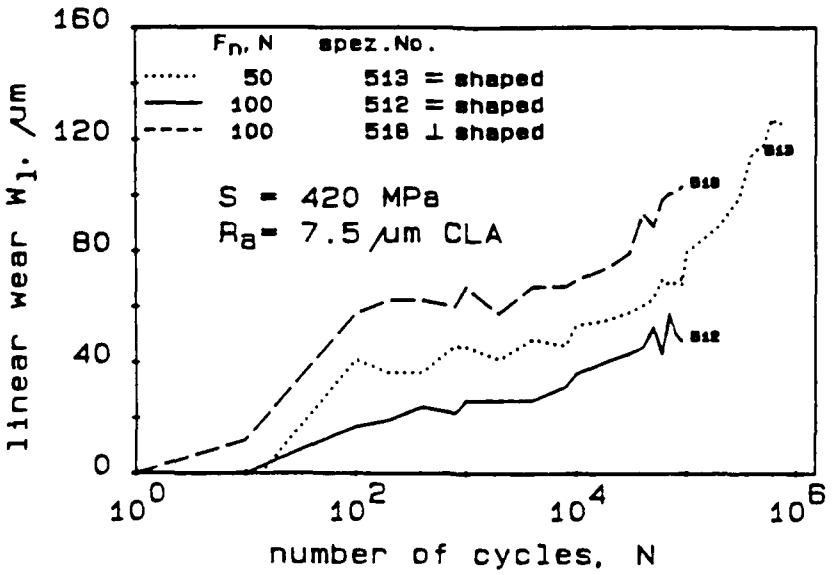

Fig.36 - Total linear wear vs. number of cycles of parallel and perpendicular shaped 480 HV specimens at normal forces of 50 and 100 N.

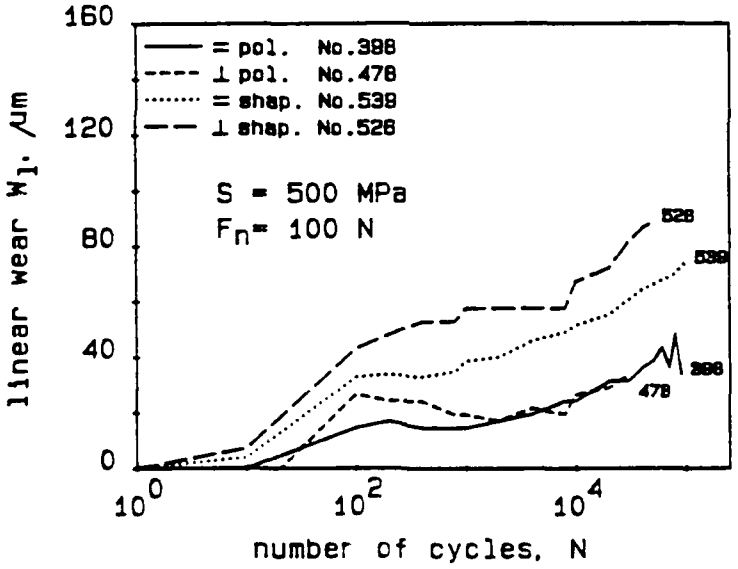

Fig.37 - Total linear wear vs. number of cycles of polished and shaped 480 HV specimens at 500 MPa fatigue load and 100 N normal force.

of the pad.

The ratios of the final linear wear of the pad to the final total linear wear, calculated from wear scar diameter, weight loss of the pad and total wear, are shown in Table 3.1 for polished and shaped 480HV specimens. The calculated values are the average from several tests. It can be noticed, that the influence of the normal force is low for polished specimens and that a distinct effect is present for the shaped specimens.

Table 3.1

Ratio of the pad wear to the total wear calculated from wear scar diameter, weight loss and total wear.

F_n, N	$w_{1,pad}/w_{1,total}$, %			
	polished		shaped	
	∥	⊥	∥	⊥
50	71	67	52	46
100	71	65	55	63
200	70	52		

3.4 Electrical contact resistance

3.4.1 Average resistance

The average contact resistance was used to monitor the development of fretting damage in the contact zones. The wear debris and oxides that accumulate in the contact zone in the form of a highly localized, thick and insulating layer can lead to a rapid increase in contact resistance and consequently, to a virtually open circuit.

Fig.38 illustrates typical contact resistance behaviour of parallel and perpendicular polished 480 HV specimens at 420 MPa fatigue load and 100 N normal force. To correlate the electrical contact behaviour to the fretting process, the simultaneously measured linear wear and friction force is also plotted. For both directions of surface polishing the resistance is lower than 10 ohms during the first

10exp4 to 10exp5 cycles. After this nearly metallic contact behaviour the resistance rises rapidly to high values and fluctuates considerably. Concomitant to the fluctuations of the resistance, variations of the tribological parameters, linear wear and friction force, appear. The region of loading cycles, where the fluctuations appear, is the region of life time, where the oxide produced during fretting begins to perform an important action: At this point of life time the wear mechanism changes from two-body abrasion to three-body abrasion because of the presence of oxide debris, or adhesion is limited by the oxid layer at an interface. The action of the fretting debris begins one decade earlier in the case of the parallel polished specimens than in the case of the perpendicular polished specimens.

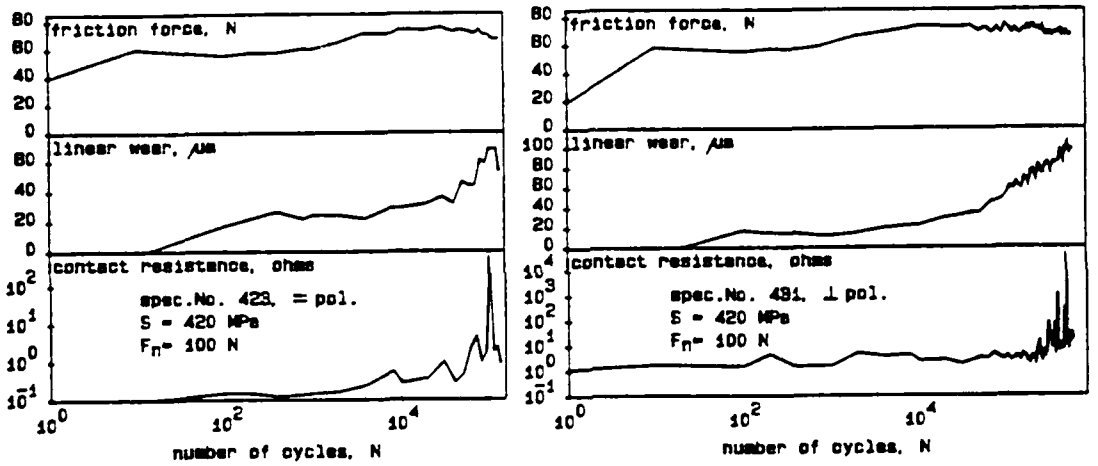

Fig.38 - Contact resistance, linear wear and friction force vs. number of cycles of parallel and perpendicular polished 480 HV specimens at 420 MPa fatigue load and 100 N normal force.

The shaped specimens show a similar behaviour of the contact resistance which is presented in Fig.39. During the first three decades of the number of cycles the resistance remains low and the contact is metallic, but when oxide debris is formed and acts in the interface the resistance rises. The resistance

fluctuates around high values caused by local breakdown in the oxide layers. Sometimes the oxide debris can act as a lubricant so that the friction force is lowered /9/. As a result of this lubricant effect the friction force rises from the initial value, passes through a maximum, and then falls slowly at high life times.

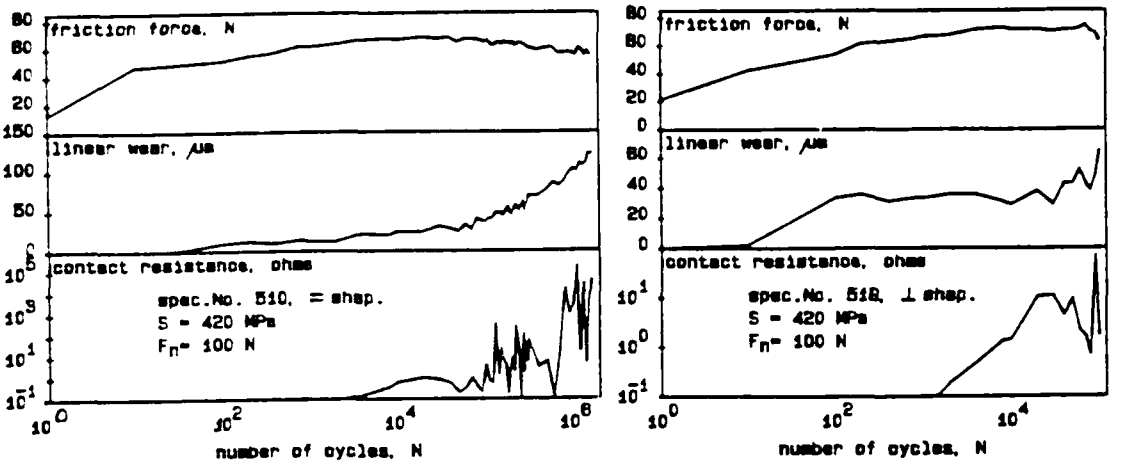

Fig.39 - Contact resistance, linear wear and friction force vs. number of cycles of parallel and perpendicular shaped 480 HV specimens at 420 MPa fatigue load and 100 N normal force.

3.4.2 Instantaneous resistance

The instantaneous value of the contact resistance as a function of pad location traced during one half loading cycle while the pad moves from one reversal position to the other is shown in Fig.40-42. The value -1 on the X-axis represents the lowest pad position when the specimen is in the maximum compression state and the value +1 represents the highest pad position when the specimen is in the maximum tension state. 0 is the position of the pad while the stress of the specimen changes sign, that is the center of the notch.

Fig.40 shows the profiles of contact resistance of a parallel polished 480 HV specimen. The value of

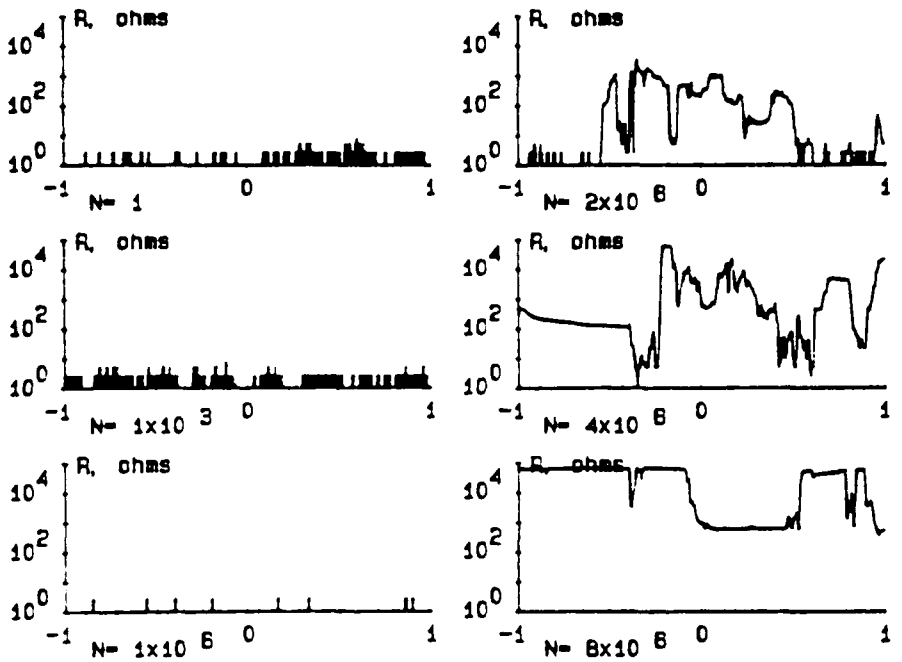

Fig.40 - Instantaneous contact resistance vs. pad position of a parallel polished 480 HV specimen at 400 MPa fatigue load and 100 N normal force. Specimen No. 399, roughness 0.48 μm CLA, slip amplitude 35 μm.

the resistance throughout the first 1/8 of the life time is relatively low, indicating that there is always substantial metal-to-metal contact. For the remainder of the life time there is a rise to high values due to fretting debris. Preferential near to the reversal positions of the pad metallic contacts appear.

The contact resistance of hard 840 HV specimens, polished parallel and perpendicular to the sliding direction, is shown in Figures 41-42. The transition from the low metallic contact at the beginning of the test to the high resistance contact appears earlier for the parallel polished specimen than for the perpendicular polished one. The perpendicular polished specimen which has lower values of resistance shows numerous events of metallic contact during the whole life time. For both specimens the contact resistance

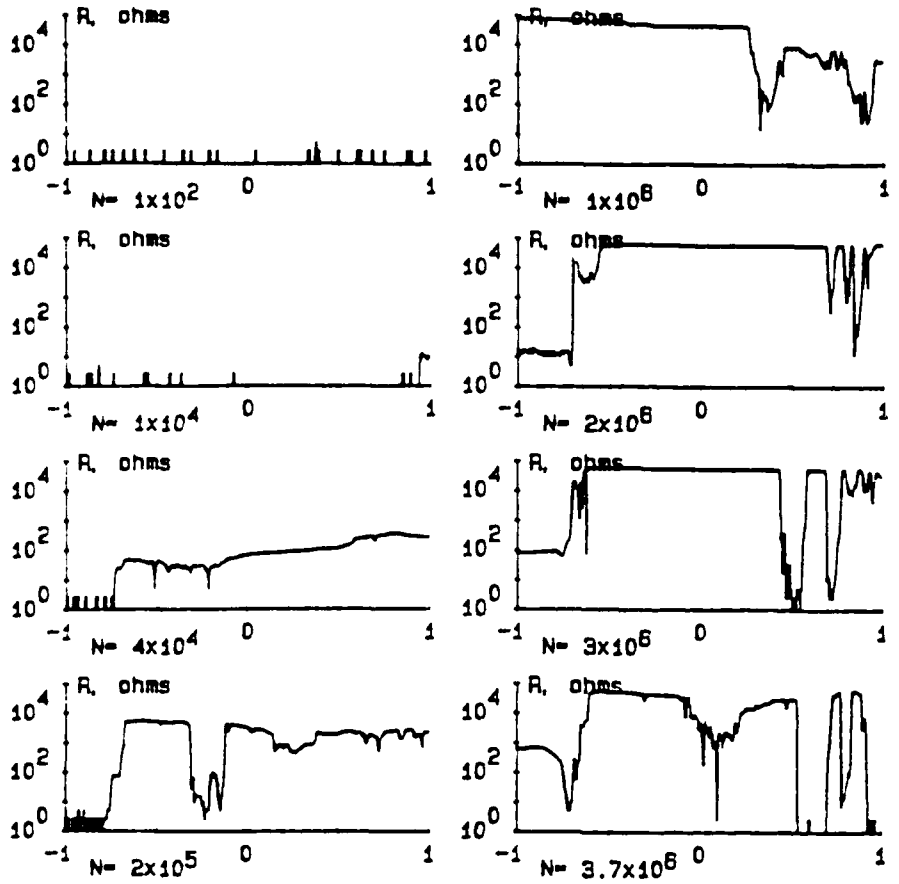

Fig.41 - Instantaneous contact resistance vs. pad position of a parallel polished 840 HV specimen at 600 MPa fatigue load and 100 N normal force. Specimen No. 332, roughness 0.41 μm CLA, slip amplitude 75 μm.

may differ by orders of magnitude between the ends and the center of a fretted track where insulating debris tends to accumulate.

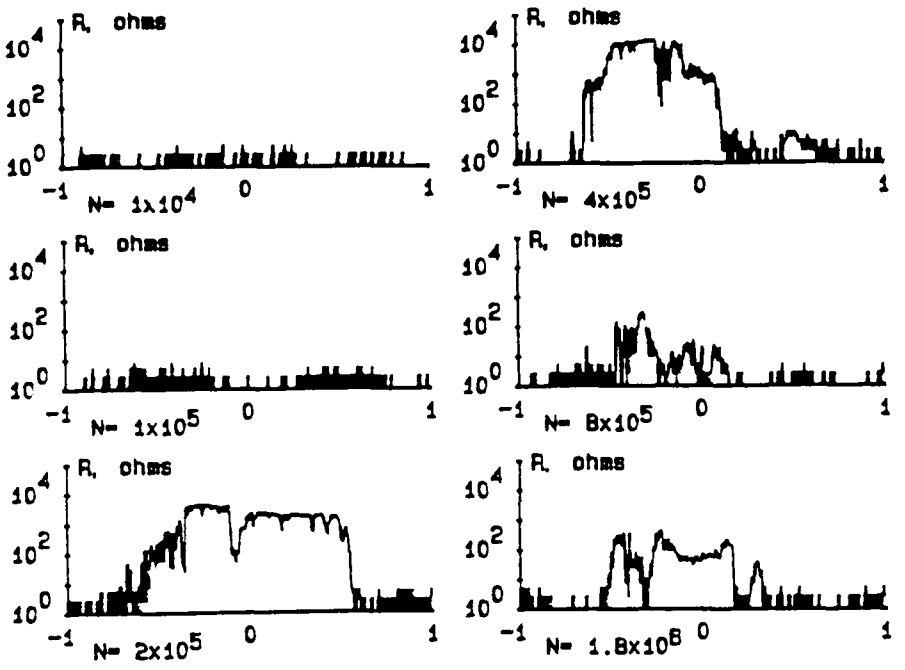

Fig.42 - Instantaneous contact resistance vs. pad position of a perpendicular polished 840 HV specimen at 600 MPa fatigue load and 100 N normal force. Specimen No. 344, roughness 0.58 µm CLA, slip amplitude 75 µm.

3.5 Magnetic induction voltage

The simplest way for crack detection by the magnetic method is to measure the r.m.s. voltage which is induced in the pick-up coil during the experimental run. A typical curve of the inductive r.m.s. voltage as a function of the number of loading cycles is shown in Fig.43. The left diagram shows a monotonic decrease of the induction voltage during the whole test duration due to the demagnetization of the specimen caused by the cyclic stressing. At the end of the curve a rapid voltage drop appears due to crack growth. This voltage drop is presented in the right diagram on a large scale. The plotted measuring points are only those values which were stored on

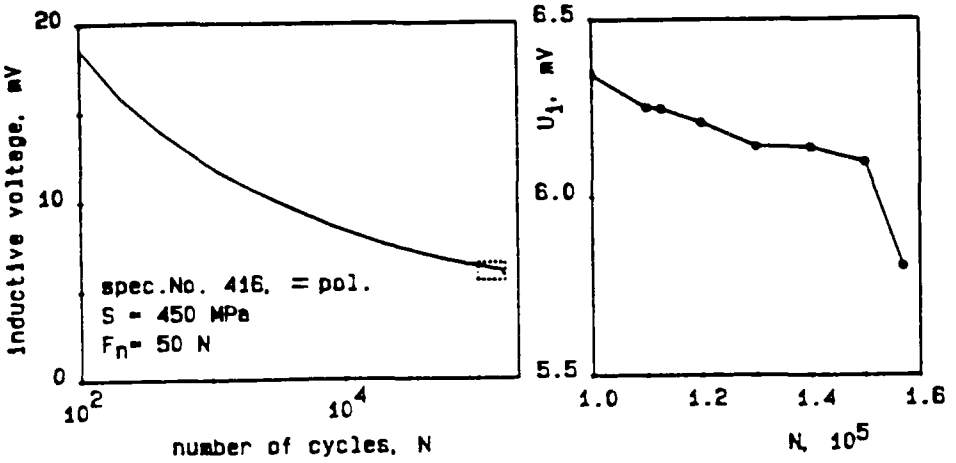

Fig.43 - Induction voltage for crack growth detection vs. number of loading cycles of a parallel polished 480 HV specimen at 450 MPa fatigue load and 50 N normal force. Specimen No. 416.

tape for later plotting. To detect the crack nucleation during the test run the inductive voltage was continuously measured.

Another more sensitive method for crack growth detection which needs however a high capacity for measuring and processing the aquired data is the measurement of the instantaneous induced voltage as a function of time during a load cycle. Changes of the shape of the curves, gathered at different life times are detectable by the method of single frequency discrete Fourier analysis. The curves of induction voltage and the resulting spectra of amplitude belonging to different numbers of loading cycles are shown in Fig.44. The starting point of the voltage curves is the crossover point of the loading function.

As long as no crack is present the amplitude of the curves decreases due to demagnetization but the profiles remain similar. Within the interval of load cycles in which the nucleation and growth of a crack takes place, the shape of the induction voltage curve is changed which is clearly reflected by the spectra of amplitudes. Each spectrum contains the values of

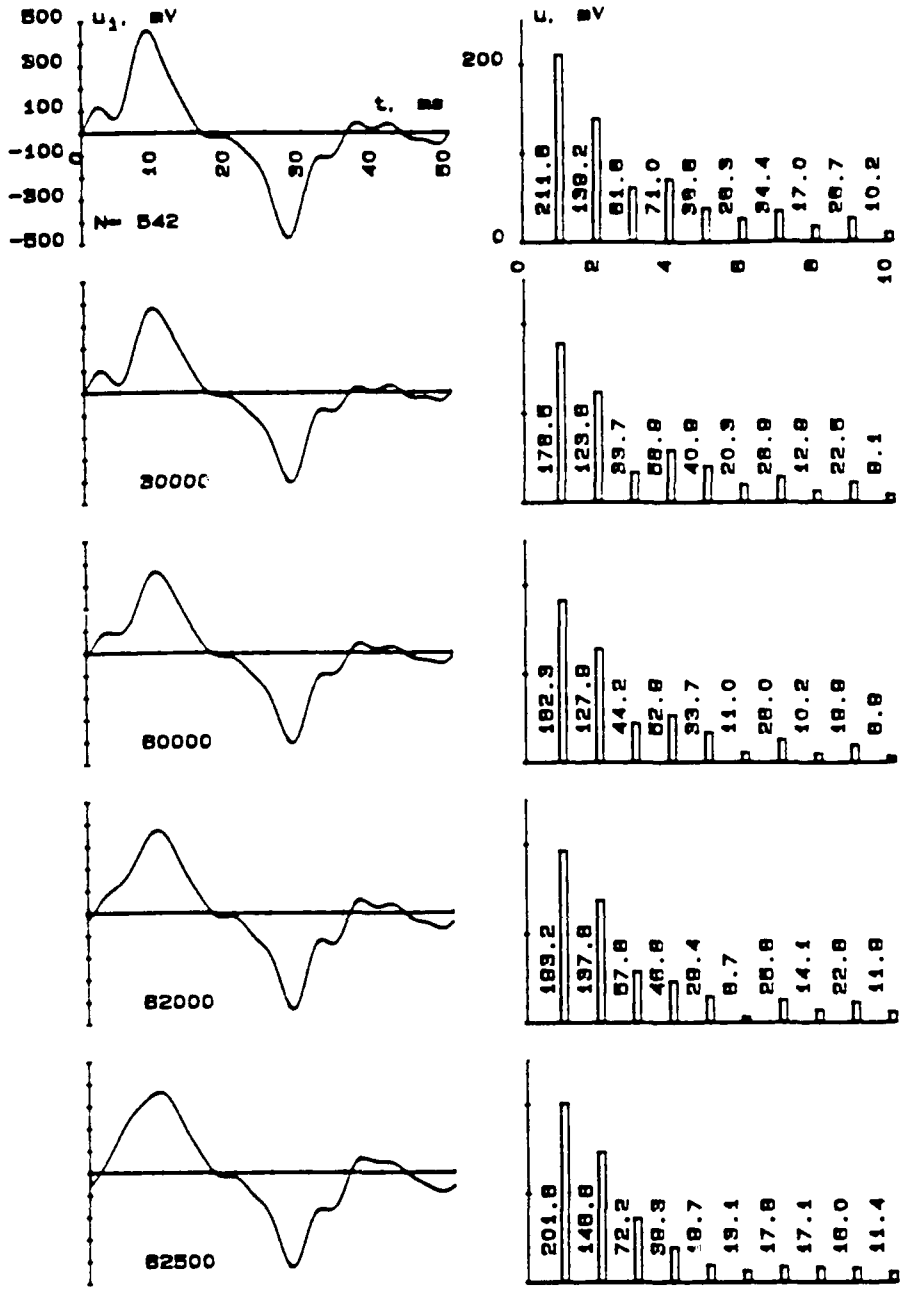

Fig.44 - Instantaneous induction voltage during a loading cycle and Fourier spectrum of amplitude of a parallel polished 480 HV specimen at 450 MPa fatigue load and 50 N normal force. Specimen No. 406.

the amplitudes of the first 10 harmonics.

The amplitude values of the first five harmonics of the induction voltage as a function of loading cycles are plotted in Fig.45. All curves show a rapid change -increase or decrease- at their ends which indicates the crack development.

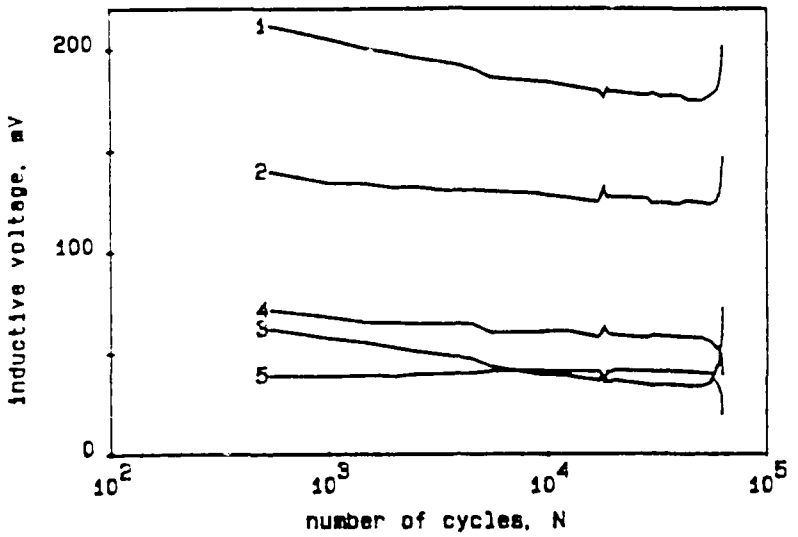

Fig.45 - Amplitude values of the first 5 harmonics of the Fourier spectrum of the induction voltage vs. number of loading cycles of a 480 HV specimen at 450 MPa fatigue load and 50 N normal force. Specimen No. 406.

3.6 Contact temperature

The used method of temperature measurement was not satisfactory because the specimens were heated by the hydraulically actuated grips of the servo hydraulic testing machine so that only sometimes at high normal forces a small fretting initiated heating effect was detectable.

Fig.46 shows as a typical example the temperature of the pad and that of the shaft of the specimen during the test run. Both curves show the same tendency, a monotonic increase with increasing number of loading cycles. As the temperature of the shaft

is clearly higher than that of the notch the heatflow is directed from the shaft to the fretted notch of the specimen so that the pad temperature is mainly determined by this flow of heat.

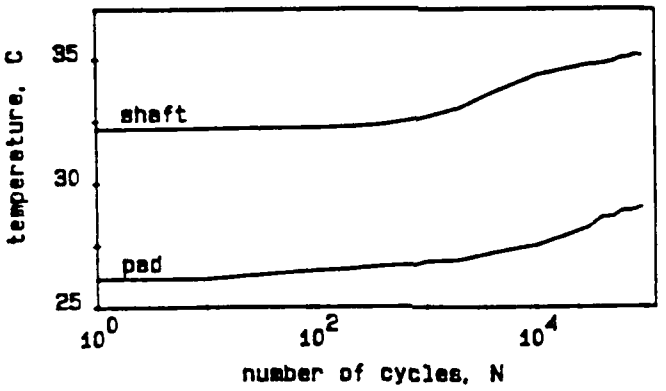

Fig.46 - Temperature of the pad and the shaft of the specimen vs. number of loading cycles of a perpendicular shaped specimen at 420 MPa fatigue load and 100 N normal force. Specimen No. 518.

3.7 Stress conditions under fretting fatigue

Fatigue cracks can be initiated under relatively low stresses at surface imperfections. Imperfactions from machining marks and surface damage are the most serios types. In normal service, the stress concentrations at surface imperfections are initially not severe enough to produce catastrophic failure. But under the influence of a sliding fretting contact stresses of sufficient intensity may be induced to cause plastic deformation. Because of this irreversible deformation, even those surfaces which are initially mirror smooth may develop surface irregularities that can initiate cracks after a sufficient number of stress cycles. Usually in a ductile material the crack tips are not sharp enough to produce catastrophic failure, however, they are sufficient to cause slow propagation of a crack into the material. Eventually the crack may become sufficiently deep so

that the stress concentrations exceed the fracture strength and catastrophic failure occurs. The two steps of crack growth and final fracture may be identified on the fracture surface (Fig.17).

The feature of the fretting fatigue phenomenon is that the contact region of the specimen is subjected to more general loading than the uniaxial cyclic loading and that the nominal stress of the fatigue loading may not be the significant stress for the occurrence of mechanical failure by fracture. The specimen is subjected to a system of triaxial stresses arising from the friction- and normal force of the contacting pad and the cyclic axial loading. The magnitude of the shear stress, which arises as a result of relative motion of the fretting pad with respect to the specimen, will depend on the degree of adhesion or the coefficient of friction between the surfaces /10,11/.

For the dimensioning of parts or specimens which will be cyclically stressed under fretting fatigue conditions it will be useful to have a correlation between fretting fatigue under combined stresses and that in uniaxial fatigue loading. To achieve such a correlation criterion it is usually assumed that the material is mechanically isotropic and deforms plastically at constant volume. In assuming plastic isotropy, macroscopic shear is allowed to take place along lines of maximum shear stress, and crystallographic slip is ignored.

As the presence of a shear stress is essential for the occurrence of plastic deformation, the slip plane in a small element within the surface of the specimen, which is inclined at 45 degree to the axis of the specimen, is considered. The resolved shear stress has a maximum value in this slip plane.

According to the principle of superposition, the stress at any point of the specimen can be found as a sum of components coming from the axial stress, the tangential stress and the stress due to the normal force. Cracking and failure is assumed to occur when the sum of the alternating shear stress amplitude acting in the considered slip plane exceeds the fatigue strength. The fatigue strength in shear is assumed to be half the value of the fatigue limit.

The stress which must be calculated is the maximum shear stress occurring in the vicinity of the contact region. This stress is not computed simply on the basis of the normal load but also include the effect of the friction force. Two types of contact appear during a fretting fatigue test: during the initial phase the contact is Hertzian case cylinder on a flat and after some thousends of loading cycles the contact is a conforming one which can be considered to be a flat on a flat.

The relations for the estimation of the maximum shear stress caused by the action of the fretting pad is given by the relations (3.1) to (3.7) for the test geometry cylinder on a flat and the sliding perpendicular to the axis of the cylinder /12/. The case of a cylinder on a flat is a limiting case of parallel cylinders, with one of the cylinders having an infinite radius. The value of K assumed should be appropriate for sharp edges and corners. Since the edges associated with the pads are not sharp, K is taken to be

Hertzian case:

$$\tau_{max} = K \left(\frac{1 + \mu}{2} \right) q_0 \qquad (3.1)$$

$$q_0 = \frac{2}{\pi} \frac{P}{Lb} \qquad (3.2)$$

$$b = 2\sqrt{\frac{2PR}{L} \frac{(1-\nu^2)}{\pi E}} \qquad (3.3)$$

$$\tau_{max} = 17.07\ K (1+\mu) \sqrt{P} \qquad (3.4)$$

conforming geometry:

$$\tau_{max} = K\sqrt{\frac{1}{4} + \mu^2}\ q_0 \qquad (3.5)$$

$$q_0 = \frac{P}{Lb} \qquad (3.6)$$

b= experimental value

$$\tau_{max} = 0.2\ K \frac{P}{b}\sqrt{\frac{1}{4} + \mu^2} \qquad (3.7)$$

(3.4), (3.7): P [N], τ_{max} [MPa]

Symbols:

μ= coefficient of friction
ν= Poisson's ratio
E= Young's modulus
K= stress concentration factor
τ_{max}= maximum shear stress
q_0= maximum contact pressure
P= normal load
R= radius of cylindrical pad
L= length of cylinder
b= width of contact area

from the order of 1. The values of the friction coefficient will be calculated using the experimental values of friction force and normal force. The equations 3.4 and 3.7 follow from the equations 3.1 and 3.5 with the material constants of steel and the dimensions of the specimen-pad system.

The effective shear stress in the considered 45 degree slip plane of the slipped surface region of the specimen is given by the sum of the shear stress resulting from the applied alternating stress and the additional stress in the surface due to the fretting contact which is greater the higher the coefficient of friction and the pressure are.

During the initial phase of a fretting fatigue test the additional shear stress derived from equation 3.4 may be relatively high compared with the shear stress resulting from the fatigue loading. At high normal forces this is also the case for low cofficients of friction. These conditions of high

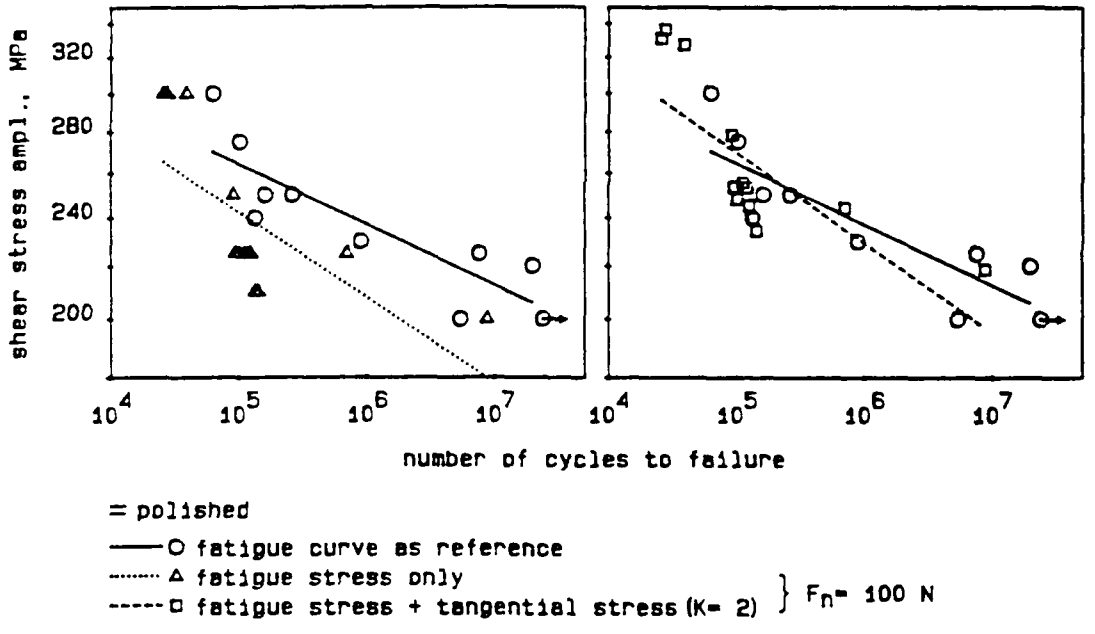

Fig.47 - Effective shear stress versus number of cycles to failure of parallel to the sliding direction polished 480 HV specimens at a normal force of 100 N.

shear stress in the slip plane may be advantageous for the nucleation of cracks.

At higher numbers of cycles the Hertzian case becomes insignificant and the additional maximum shear stress is given by equation 3.7 of the conforming contact geometry. As the coefficient of friction is then relatively high, the condition for the nucleation and growth of cracks may also be advantageous during the main part of the live time.

To show the utility of these considerations two examples of fretting fatigue tests are represented. The Figures 47-48 show the shear stress as a function of the number of loading cycles of a parallel and a perpendicular to the sliding direction polished 480 HV specimen. Each Figure contains two diagrams: the left diagram shows the alternating shear stress acting in the 45 degree slip plane without consideration of the fretting influence versus the number of cycles. The right diagram shows the effective shear

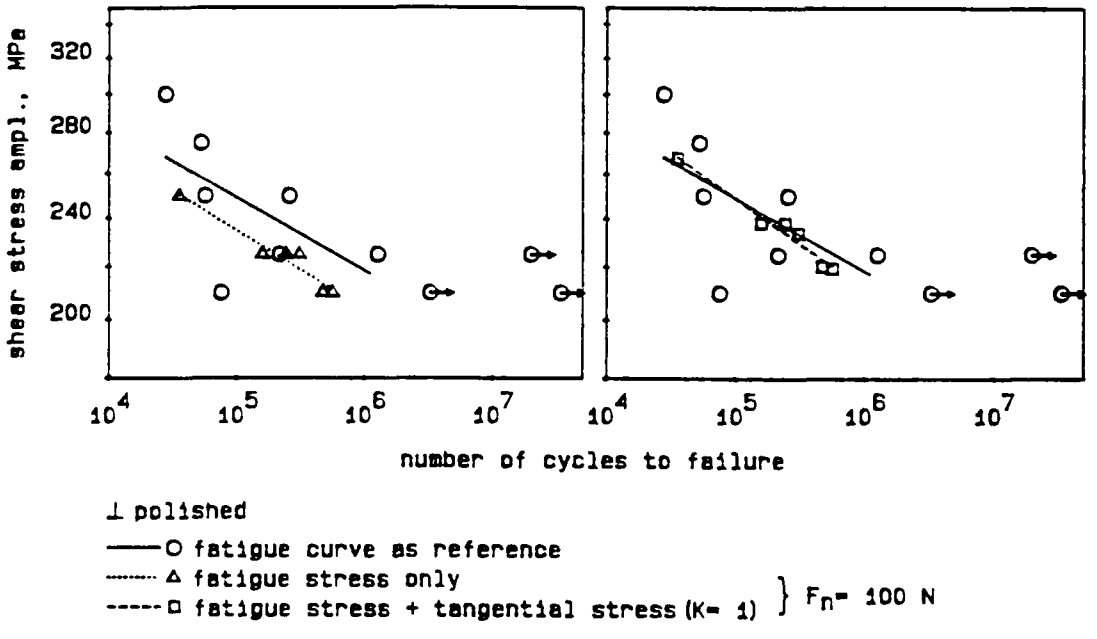

Fig.48 - Effective shear stress versus number of cycles to failure of perpendicular to the sliding direction polished 480 HV specimens at a normal force of 100 N.

stress with consideration of the shear stress arising from the friction force derived from equation 3.7. As a reference the fatigue curve in the absence of fretting is plotted in both diagrams. The left diagrams of Figures 47-48 are equivalent to the Figures 9-10. For the calculation of the shear stress from equation 3.7 the maximum value of u, taken from experiment, is used. For the width b of the contact area half of the experimental value, which was determined at the end of each experiment, is used. The stress concentration factor is set to 2 for the parallel polished specimens and it is set to 1 for the perpendicular polished specimens.

The consideration of the friction force for the calculation of the effective shear stress moves the fretting fatigue curves so to higher stress values, that they are in reasonable good agreement with reference to the fatigue curve without fretting (right diagrams). That means that the fretting fatigue limit or strength can be estimated from the corresponding uniaxial fatigue limit or strength merely by replacing the fatigue shear stress by the effective shear stress which is the sum of the fatigue stress and the stress due to fretting. This is useful for the engeneering designer which needs at the preliminary design stage a method of estimating the behaviour of a component under fretting fatigue conditions.

4. Conclusions

(1) A test equipment for fretting fatigue experiments was developed, which allows the simultaneous measurement of numerous experimental parameters. The normal force is generated by an electromagnetically driven device under closed loop control so that it is highly constant during the experimental run.

(2) Programs for computer aided data aquisition and analyses of experimental parameters has been developed. The computer aid has been shown to be essential for the largely automatic control of the tests.

(3) A method for the nondestructive detection of damage (cracks) in an early stage based on magnetic induction measurements has been developed and varified.

From the experimental and analytical results, the following conclusions were obtained:

(4) There is a definite decrease in life owing to fretting fatigue by both polished and shaped specimens.

(5) The reduction in fatigue strength of the perpendicular to the sliding direction polished specimens is greater than that of the parallel to the sliding direction polished specimens. The reduction of fatigue strength increases with increasing normal force.

(6) The relative high dispersion of the S/N curve obtained by fretting fatigue tests is larger at the higher surface roughness of the shaped specimens.

(7) For the group of the shaped specimens a similar to (5) statement of the effect of the shaping direction on the fatigue strength is not possible on account of the fluctuations.

(8) Cracks usually develop from the surface of the specimen in the region of contact. Surface cracks outside of the fretting region were sometimes observed preferentially on perpendicular to the sliding direction polished and shaped specimens.

(9) Comprehensive information of the fretting process which influence the fatigue behaviour is obtainable by comparison of the simultaneously measured parameters: friction force, normal force, linear wear rate and electrical contact resistance.

(10) The effective shear stress in the contact region of the specimen may be used to clarify the early stage fatigue cracks initiation and propagation.

Acknowledgments

This study was sponsered by the European Research Office of the U.S. Army (ERO), London, U.K., and the author is grateful for this agency's support.
The author also thanks Lothar Scherpinski for his help in experiments.

References

/1/ Waterhouse, R.B., "Fretting Corrosion", Pergamon Press, Oxford, 1972.

/2/ Waterhouse, R.B., "Fretting Fatigue", Applied Science, London, 1981.

/3/ Bill, R.C., "Fretting Wear and Fretting Fatigue-How are they related?", Journal of Lubrication Technology 105(1983)230-238

/4/ Hoeppner, D.W., "Fretting Fatigeu Considerations in Engineering Design", Wear, 70(1981)155-164

/5/ Sander,H., "Multitechnique Studies on Fretting Fatigue: Influence of Surface Treatment", First Annual Technical Report, 1984, AD R+D 4038-AN

/6/ Sander,H., "Multitechnique Studies on Fretting Fatigue: Influence of Surface Treatment", Second Annual Technical Report, 1985, AD R+D 4038-AN

/7/ Günther, W., "Schwingfestigkeit", VEB Deutscher Verlag für Grundstoffindustrie, Leipzig 1973

/8/ Weibull, W., "Fatigue testing and analysis of results", Pergamon Press, Oxford 1961

/9/ Halliday, J.S. and W. Hirst, "The fretting corrosion of mild steel", Proc. R. Soc. London, Ser. A, 236(1956) 411-425

/10/ Switec, W., "Early stage crack propagation in fretting fatigue", Mechanics of Materials 3 (1984)257-267, North-Holland

/11/ Broszeit, E., F.J. Heß and K.H. Kloos, "Werkstoffanstrengung bei oszillierender Gleitbewegung" (Materials stressing at oscillating sliding movements), Z. Werkstofftech. 8 (1977)425-432

/12/ Bayer, R.G. and Ku, T.C., Handbook of analytical design for wear, Plenum Press New York 1964